THIS DOCUMENT PROVIDED BY THE ABBOTT AEROSPACE
TECHNICAL LIBRARY
ABBOTTAEROSPACE.COM

R. & M. No. 3559

R. & M. No. 3559

MINISTRY OF TECHNOLOGY

AERONAUTICAL RESEARCH COUNCIL
REPORTS AND MEMORANDA

Comparative Theoretical Calculations of Forces on Oscillating Wings through the Transonic Speed Range

By H. C. Garner and Doris E. Lehrian

LIBRARY
ROYAL AIRCRAFT ESTABLISHMENT
BEDFORD.

LONDON: HER MAJESTY'S STATIONERY OFFICE
1969
PRICE £1 4*s.* 0*d.* NET

THIS DOCUMENT PROVIDED BY THE ABBOTT AEROSPACE
TECHNICAL LIBRARY
ABBOTTAEROSPACE.COM

Comparative Theoretical Calculations of Forces on Oscillating Wings through the Transonic Speed Range

By H. C. Garner and Doris E. Lehrian

Reports and Memoranda No. 3559*
August, 1967

Summary.

Three planforms, rectangular, delta and symmetrical tapered, have been selected for combined theoretical and experimental aerodynamic research. Numerous linearized theoretical methods have been applied to each planform in oscillatory pitching and plunging motion at subsonic, sonic and supersonic Mach numbers. After a brief review of available theories, the calculated and measured data are presented. For each wing, separately, the lift and moment derivatives are studied as functions of Mach number, frequency parameter and pitching axis. It is found possible to link results from the various theories approximately by continous curves against Mach number for fixed values of the frequency parameter. Satisfactory comparisons with experiment are found in purely subsonic or supersonic flow, but in the transonic region uncertainties of tunnel-wall interference may mask the true discrepancies due to wing thickness and other non-linear disturbances. With the aid of exact or analytical theories for the particular wings, seven general theoretical methods have been appraised. Finally an attempt is made to review the status of linearized theory in the narrow transonic range where effects of frequency and Mach number become very large.

CONTENTS

*Replaces N.P.L. Aero. Report 1246—A.R.C. 29 367.

THIS DOCUMENT PROVIDED BY THE ABBOTT AEROSPACE
TECHNICAL LIBRARY
ABBOTTAEROSPACE.COM

CONTENTS—*continued*

1. *Introduction.*

The theoretical prediction of oscillatory wing loading is a necessary preliminary to flutter calculations. Generalized aerodynamic forces in rigid and elastic modes must be determined theoretically to ensure adequate flutter margins. In most applications linear theories are used, and the accuracy of such methods has been constantly under review. This has led on the one hand to mathematical or numerical improvements within the linear framework, and on the other to comparative measurements. For practical reasons experimental aerodynamic forces are largely restricted to rigid modes, and when comparisons are successful greater reliance can be placed on the theoretical derivatives for elastic modes.

There is reasonable confidence in calculations by linearized lifting-surface theory as applied to oscillating wings at low subsonic and high supersonic speeds. Moreover, it is shown in Ref. 1 (Acum and Garner, 1961), that for rigid pitching modes the derivatives are fairly well predicted by linear theory at Mach numbers below 0·8 and above 1·4; in the sub-critical range discrepancies between theory and experiment tend to be systematic, and in the upper supersonic range they can often be reduced to acceptable limits by a simple correction for wing thickness. Experimental information for lower supersonic speeds is scanty, while that in the upper subsonic and transonic range may be subject to uncertainties in tunnel-wall interference and restricted to rather low values of the frequency parameter. At the same time the assumptions of linear theory become increasingly restrictive as sonic Mach number is approached; moreover, there are important effects of wing thickness and shock waves beyond the scope of oscillatory theories.

Nevertheless, a firm theoretical basis is necessary to bridge the transonic speed range. However restrictive and difficult linear theory may become, it retains some significance. A preliminary objective for any understanding of the behaviour of transonic oscillatory forces is the establishment of complete theoretical curves of pitching derivatives against Mach number for a range of fixed values of the frequency

THIS DOCUMENT PROVIDED BY THE ABBOTT AEROSPACE
TECHNICAL LIBRARY
ABBOTTAEROSPACE.COM

parameter. The purposes of the present investigation are to discover to what extent this can be achieved with particular reference to general theoretical methods, and to examine the relevant experimental data. The three planforms of Fig. 1, selected from the NPL experimental programme, cover many facets of the problem. Measurements on the rectangular and symmetrical tapered wings have been made, but unfortunately the experimental rig for testing the delta wing at transonic speeds was never completed.

The rectangular wing of aspect ratio 2 is an obvious choice in view of the large amount of analytical and numerical work done on it; the theoretical difficulties are acute in the low supersonic range. The complete delta wing of aspect ratio 1·5 is fairly representative of current thought for high-speed aircraft; it is well covered by theoretical work especially at sonic and supersonic speeds, but the high subsonic range poses the greatest theoretical challenge. The symmetrical tapered planform provides a fairly high aspect ratio 4·33 with a fair degree of taper and is chosen because it can be treated by established theoretical methods for general frequency outside a small range of low supersonic Mach number. At low supersonic speeds in our present range of interest, the first two planforms have leading edges which are respectively always supersonic and always subsonic, whilst for the third planform the leading edge becomes sonic within the range. This is illustrated in Fig. 2; the Mach lines at $M = 1{\cdot}075$ indicate the relative complexity of the theoretical problems for the three wings.

Available subsonic, sonic and supersonic theories are discussed separately in Sections 2.1, 2.2 and 2.3. At low supersonic speeds the need arose for a general method applicable to the widest practical range of planform and frequency parameter, and such a method was programmed at Hawker Siddeley Aviation Limited (Kingston) under contract to the Ministry of Aviation. The investigation has also demanded a large amount of computational work, some of which was carried out at the de Havilland Division of Hawker Siddeley Aviation Limited and the South Marston Works of Vickers-Armstrongs (Engineers) Limited under M.o.A. contract; there has also been close collaboration with the Structures Department of the Royal Aircraft Establishment. The provision of theoretical and experimental results is discussed in Sections 3.1 and 3.2, where the sources of data are acknowledged.

Sections 4, 5 and 6 describe the numerical results for each planform in turn. Acum[2] (1962) has already given an account of the calculations and measurements that existed at the time. A greater understanding of the various sources of error has led us to reject some of the data. For the rectangular wing in particular, the measurements at the higher frequencies are invalidated by model distortion, and those at subsonic Mach number require large corrections for slotted-wall interference, which have recently been formulated. The prospects of the general theoretical methods for subsonic and supersonic speeds are assessed in Sections 7.1 and 7.2, while in Section 7.3 an attempt is made to appraise their status in the problematical transonic speed range. Some general conclusions may be drawn from the investigation (Section 8); some fields for possible future theoretical and experimental developments have been exposed.

2. *Theoretical Background.*

2.1. *Subsonic Flow.*

With very few exceptions, solutions by subsonic lifting-surface theory are calculated by collocation methods in which the boundary conditions are applied at a finite number of points inside the planform. The linearized integral equation over the planform area S

$$\frac{w(x,y)}{U} = \int_S \int l(x',y')\, K(x-x', y-y', M, \omega)\, dx'dy' \tag{1}$$

relates the upwash angle w/U to the non-dimensional wing loading l. The kernel K, a rather complicated function of streamwise and spanwise distances, Mach number and frequency of oscillation, is discussed at length by Williams[3]. He has derived equation (1) and has reviewed the theoretical problems that it poses.

The kernel function in equation (1) simplifies considerably when the frequency ω is small. Multhopp's theory, described in Ref. 4, applies to this limiting case. The general treatment of equation (1) for arbitrary

THIS DOCUMENT PROVIDED BY THE ABBOTT AEROSPACE
TECHNICAL LIBRARY
ABBOTTAEROSPACE.COM

frequency was pioneered by Watkins *et al*[5] and has been developed subsequently by many authors. Refs. 6 to 8 differ in detail but are very similar in principle. Richardson's[6] method, being somewhat more convenient for calculation, was the first to be programmed for a digital computer and has been used extensively in the aircraft industry. It is, however, less accurate than Acum's[7] method which is not yet fully programmed. In Ref. 8, Davies has combined the greater accuracy of Ref. 7 with the speed of a fully mechanized Mercury programme; nevertheless, there are limitations imposed by the capacity of the computer, which may be more important than was at first thought (Section 7.1). All these collocation methods apply to a wide range of planform.

In Fig. 3, the delta wing in pitching and plunging motion is used to illustrate some features of the methods of Refs. 4 and 7. The wing is defined by its leading edge $x_l(y)$, chord $c(y)$ and semi-span s. The collocation points (x_{pv},y_v) are defined by

$$x_{pv} = x_{lv}+\tfrac{1}{2}c_v\left[1-\cos\frac{2\pi p}{2N+1}\right], p = 1,2,\ldots N \tag{2}$$

and

$$y_v = s\sin\frac{v\pi}{m+1}, v = 0, \pm1,\ldots \pm\tfrac{1}{2}(m-1), \tag{3}$$

where $x_{lv} = x_l(y_v)$, $c_v = c(y_v)$, m is an odd integer denoting the number of collocation sections, and N is the number of collocation points at each section. Fig. 3a shows their arrangement for the combination $m(N) = 11(3)$.

In the chordwise direction the wing loading $l(x',y')$ includes N terms of a Fourier series. Then, to avoid a logarithmic infinity in upwash from the double integral of equation (1) at $v = 0$, the apex of the planform is rounded so that in equation (2)

$$\left.\begin{aligned} x_{l0} &= \frac{5}{6}x_l(0)+\frac{1}{6}x_l(y_1)\\ c_0 &= \frac{5}{6}c(0)\ +\frac{1}{6}c(y_1)\end{aligned}\right\}. \tag{4}$$

The artifice of equation (4) is not used in Ref. 8, since Davies conveniently replaces equation (3) by

$$y_v = s\cos\frac{v\pi}{m+1}, v = 1,2,\ldots m \tag{5}$$

where m is even, thereby eliminating the problem of collocation points on the centreline. Nevertheless, there remains an implicit logarithmic singularity at $y = 0$, and it is unknown whether the method of Ref. 7 or 8 is preferable in this respect. Richardson's[6] method is programmed to include odd or even values of m.

2.2. *Sonic Flow.*

One of the earliest theories for an oscillating three-dimensional wing at $M = 1$ is due to Mangler[9] (1952). He gives the leading terms of the analytical solution for a complete delta wing, which suffice for small values of the frequency parameter. The developments in sonic lifting-surface theory are examined in Refs. 10 and 11. The two mathematical treatises are to some extent complementary, since Landahl[10] is primarily concerned with his contributions to the analytical theory of rectangular and delta wings, while Davies[11] also describes a collocation method for arbitrary planform.

In Chapter 3 of Ref. 10, Landahl gives a solution in series for delta wings. This extension to the theory of Ref. 9 applies if the product of the aspect ratio and the square root of the frequency parameter is not too large: we write

THIS DOCUMENT PROVIDED BY THE ABBOTT AEROSPACE
TECHNICAL LIBRARY
ABBOTTAEROSPACE.COM

$$A^2\bar{\nu} < 1\,, \tag{6}$$

where in terms of geometric mean chord $\bar{c}$

$$\left.\begin{aligned} A &= 2s/\bar{c} \\ \bar{\nu} &= \omega\bar{c}/U \end{aligned}\right\}. \tag{7}$$

Chapters 4, 6 and 7 of Ref. 10 describe separate theories for oscillating rectangular wings at $M = 1$. The first leads to an expansion in powers of aspect ratio and frequency parameter; as for the corresponding theory for the delta wing in Chapter 3, the condition (6) restricts calculations to fairly low values of either A or $\bar{\nu}$. The second of Landahl's theories is essentially for high aspect ratios when the interaction between the side edges can be ignored; it is the simplest of the three and gives fair accuracy provided that $A^2\bar{\nu}$ is large (> 2, say). The third theory is exact but would require unlimited computation; in practice, it reduces to the second theory with an additional term which is amenable to automatic computation. The parametric restriction

$$A^2\bar{\nu} > 1 \tag{8}$$

seems reasonable, so that for rectangular wings Chapters 4 and 7 of Ref. 10 might be expected to cover the whole range of aspect ratio and frequency.

The collocation method of Davies[11] has many of the features of those in use for subsonic flow. The governing differential equation is simplified by the substitution $M = 1$. A relationship similar to equation (1) is derived, and the kernel function is formulated on principles similar to those in Ref. 5. The form of load distribution $l(x',y')$ varies accordingly as the trailing edge is sonic or subsonic. Numerical solutions are again designated by the combination $m(N)$ of collocation stations across the span and chord. There is little practical restriction on planform; unlike Landahl's theories, Ref. 11 can be applied to curved planforms and has been used for the symmetrical tapered wing of Fig. 1, but the method fails if the frequency parameter is too small.

Ordinary linearized theory is based on the differential equation of sound propagation in moving co-ordinates and depends essentially on small perturbations for its accuracy. Very near $M = 1$ the perturbations from uniform flow cease to be small, however thin the wing may be, and the ordinary approximation breaks down. In Chapter 1 of Ref. 10, Landahl has suggested an alternative linear equation which will be more accurate at near-sonic speeds, provided that the frequency is not too small. The two differential equations are identical in the limit $M \to 1$. Subject to a severe condition

$$|1-M| << \bar{\nu}\,, \tag{9}$$

Landahl derives a transonic similarity law which enables his theory of Chapter 7 to be used very near to $M = 1$.

2.3. *Supersonic Flow.*

The problems of unsteady supersonic flow have been reviewed by Watkins[12]. There is a great diversity of methods ranging from exact solutions for low frequency or expansions in powers of frequency for particular wings to numerical procedures involving a box method or collocation for general planforms. Each of these approaches can play an important role at low supersonic speeds ($M < 1{\cdot}4$), where the difficulties are greatest. As already discussed and illustrated in Fig. 2, the type of planform influences the character of the problem.

For the rectangular wing some special analytical solutions are available for pitching and plunging motion. The low-frequency theory of Miles[13] covers the low supersonic range $M \leqslant 1{\cdot}118$, and the expansion to the seventh power of the frequency by Nelson *et al*[14] applies down to $M = 1{\cdot}118$; difficulties with interacting tips arise for lower Mach numbers when the frequency is not small. For the delta wing

THIS DOCUMENT PROVIDED BY THE ABBOTT AEROSPACE
TECHNICAL LIBRARY
ABBOTTAEROSPACE.COM

there is an expansion to the fifth power of the frequency by Davies[15]; although this is valid for any supersonic speed, the restriction on frequency becomes increasingly severe as Mach number decreases. An exact solution for the symmetrical tapered wing at low frequency is given in Ref. 16 and covers the range $M \geqslant 1{\cdot}035$ for which the leading edge is supersonic or sonic. Stewartson's[17] theory is general in frequency and has been programmed as a box method with a diamond grid of Mach lines subject to two conditions, that the leading and trailing edges are supersonic and that the Mach lines from the side edges do not intersect on the planform. Fig. 2 shows that the restrictions for the three planforms are respectively $M \geqslant 1{\cdot}414$, $M \geqslant 2{\cdot}848$ and $M \geqslant 1{\cdot}102$. In the present investigation this box method is only helpful for the symmetrical tapered wing.

Methods of calculating derivatives for general planforms are needed, especially for the low supersonic speed range where frequency effects are large and the solutions in Refs. 13 to 16 are inadequate. Richardson's[6] paper contains a proposal for a general collocation method in supersonic flow; a modified procedure, based on this, has been presented and programmed by Harris[18]. Allen and Sadler[19] have developed a refined box method with very little restriction on planform, frequency or Mach number. As shown in Fig. 4 for the delta wing at $M = 1{\cdot}03$, a diamond grid of Mach lines is used. Special formulae are derived for treating incomplete boxes that are intersected by the perimeter of the planform; the three types of incomplete box are differently shaded in Fig. 4 according to the number of vertices on the planform. Refs. 18 and 19 have been applied to the selected planforms, and the outcome is reviewed in Section 7.2.

3. *Pitching and Plunging Derivatives.*

3.1. *Theoretical Calculations.*

All the theoretical methods discussed in Section 2 have been used in the present numerical investigation. They are listed in Table 1 which shows the type of method, its range of applicability, and where relevant numerical results may be found. A general combination of pitching and plunging motion is represented sectionally in Fig. 3b, in which θ_0 and $\bar{c}z_0$ denote the amplitudes of pitch and plunge respectively. The oscillatory lift and pitching moment are expressed in the form

$$\left.\begin{aligned} L &= \rho U^2 S\left[\theta_0 (l_\theta + i\bar{\nu} l_{\dot{\theta}}) + z_0 (l_z + i\bar{\nu} l_{\dot{z}})\right] e^{i\omega t} \\ \mathscr{M} &= \rho U^2 S\bar{c}\left[\theta_0 (m_\theta + i\bar{\nu} m_{\dot{\theta}}) + z_0 (m_z + i\bar{\nu} m_{\dot{z}})\right] e^{i\omega t} \end{aligned}\right\}, \tag{10}$$

where the frequency parameter $\bar{\nu}$ is given in equation (7). The derivatives, defined in equations (10), may be calculated for an arbitrary pitching axis $x = x_0 = h\bar{c}$ from the formulae

$$\left.\begin{aligned} l_\theta &= A - Bh \\ l_{\dot{\theta}} &= C - Dh \\ -m_\theta &= E + Fh + Bh^2 \\ -m_{\dot{\theta}} &= G + Hh + Dh^2 \end{aligned}\right\} \tag{11}$$

and

$$\left.\begin{aligned} l_z &= B \\ l_{\dot{z}} &= D \\ m_z &= (A + F) + Bh \\ m_{\dot{z}} &= (C + H) + Dh \end{aligned}\right\}, \tag{12}$$

THIS DOCUMENT PROVIDED BY THE ABBOTT AEROSPACE
TECHNICAL LIBRARY
ABBOTTAEROSPACE.COM

where the coefficients $A,B \ldots H$ are fully tabulated for the rectangular, delta and symmetrical tapered wings in Tables 2, 3 and 4 respectively. The headings include the corresponding derivatives for a pitching axis $x_0 = 0$ through the leading edge of the root chord.

Of the calculations in subsonic flow, those by Refs. 4 and 7 have been computed at the NPL, and those by Ref. 6 are due to Bishop[20]. Davies[8] has published his $m(N) = 8(2)$ solution for the symmetrical tapered wing, and Woodcock[21] gives most of the results by Ref. 8 for the rectangular wing; those for the delta wing and the $m(N) = 12(6)$ solutions for the other two planforms have been specially computed at the RAE.

Most of the derivatives for $M = 1$ by Refs. 9 and 10 have been computed from the analytical formulae. Results from the more accurate high-frequency method in Chapter 7 of Ref. 10 are taken from Landahl's curves for the rectangular wing at $M = 1$; the corresponding solutions for $M = 0{\cdot}9$ have been received by private communication from Landahl and are used to indicate the rate of change of derivatives with Mach number near $M = 1$. Davies has sent unpublished results by his sonic theory[11] for each of the three wings.

Of the calculations in supersonic flow, those by Refs. 13 to 16 have been computed at the NPL from the published formulae and tables, and a few results for the symmetrical tapered wing by Ref. 17 are taken from solutions by method (ii) of Ref. 22. The results in Refs. 18, 19 and 22 have been supplemented to fulfil the present investigation. Harris has provided additional solutions by his theory[18] for the delta wing from the RAE Mercury computer, as have Vickers-Armstrongs on a Pegasus computer for the symmetrical tapered wing by Ref. 19. Shortly before the NPL DEUCE computer was dismantled, the box method based on Ref. 17 was applied to the symmetrical tapered wing at $M = 1{\cdot}105$ very close to its lower limit; it was also used at $M = 1{\cdot}08$ to give velocity potentials near the side edge, that were needed to check the additional solution by Ref. 19.

3.2. *Experimental Values.*

The provision of oscillatory experimental data has been hampered by uncertainties in slotted-wall interference and model distortion. Moreover, the development of a rig for testing complete models at transonic speeds was curtailed, so that anticipated results for the delta wing are lacking. Figs. 17a and 17b of Ref. 2 include direct pitching derivatives, $-m_\theta$ and $-m_{\dot{\theta}}$, measured on a half model of the rectangular wing at three frequencies. The measurements at the two higher frequencies are now considered to be unreliable due to model flexibility. A recent paper[23] claims to provide some theoretical understanding of slotted-wall interference on dynamic measurements in subsonic flow. A complete set of four measured pitching derivatives, as defined in equations (10) and (11), may be corrected to free-stream conditions by equations (58) of Ref. 23. This method of correction can be applied with some confidence, provided that the model, the frequency and the Mach number are not too large and that the three interference parameters δ_0', δ_0 and δ_1 are known. These conditions are fulfilled in the NPL measurements on half models of the rectangular and symmetrical tapered wings in the 36 in. × 14 in. tunnel with sealed slots or in the 25 in. × 20 in. tunnel with its perforated walls sealed. In normal operation, unfortunately, the former tunnel has such narrow slots that viscous effects cast doubt on the sign of the interference parameters. Similarly, as described by Moore and Wight[24], the latter perforated tunnel had uncertain characteristics due to the positioning of flaps that control the exit area from the plenum chamber to the diffuser; again, the sign of the interference is uncertain. In both cases the pitching derivatives have been left uncorrected, although the effects could be quite large. Wall interference appears to persist at low supersonic speeds, but the magnitude remains uncertain.

All the NPL experimental data to be compared with the theoretical calculations are given in Tables 5 and 6 for the rectangular and symmetrical tapered wings respectively. Some of the latter measurements have already been used in Refs. 23 and 24. The most reliable data are the corrected derivatives for $M \leqslant 0{\cdot}85$ when the ventilations are sealed, and those for the symmetrical tapered wing in the 25 in. × 20 in. tunnel with perforated walls for $M \geqslant 1{\cdot}3$ when, except for the derivative $l_{\dot{\theta}}$, the corrections are thought to be fairly small. In the speed range $0{\cdot}9 < M < 1{\cdot}1$ there are uncorrected measurements for both wings in two tunnels. The direct pitching derivatives for the symmetrical tapered wing have also been measured by Woodgate *et al*[25] in a closed supersonic tunnel for $M \geqslant 1{\cdot}38$. The rectangular half-model has an

THIS DOCUMENT PROVIDED BY THE ABBOTT AEROSPACE
TECHNICAL LIBRARY
ABBOTTAEROSPACE.COM

aerofoil section 10 per cent thick with round leading edge, but the symmetrical tapered wing, conceived as a missile control surface for supersonic flow, has a 5 per cent thick double-wedge aerofoil.

In the absence of experimental data for a delta wing of precisely $A = 1{\cdot}5$, values of the damping derivative $-m_{\dot{\theta}}$ have been taken from measurements by Orlik-Rückemann and Olsson[26] on a half model of a complete delta wing of aspect ratio 1·45 at transonic and supersonic speeds. Results for the lower of two frequencies from Fig. 9 of Ref. 26 are compared with present theoretical curves against Mach number; no interference corrections have been applied, but these are believed to be small for the pitching axis $x_0 = 0{\cdot}6c_r$.

4. *Rectangular Wing* ($A = 2$)

The theoretical pitching derivatives for the rectangular wing are illustrated by Figs. 5 to 15. These show the variation with Mach number, frequency and axis position of subsonic, sonic and supersonic solutions selected from Tables 2a, b and c respectively. Where possible, a consistent set of results is chosen from the different collocation methods, e.g., as defined in equations (2) and (3) or (5), solutions $m(N) = 11(3)$ by Refs. 4 and 7, $m(N) = 8(8)$ by Ref. 6 and $m(N) = 13(3)$ by Ref. 11. These numerical methods for general planform together with the supersonic box method of Ref. 19 are supplemented by the particular analytical solutions for rectangular wings from Refs. 10, 13 and 14.

Values of the four pitching derivatives l_θ, $l_{\dot{\theta}}$, m_θ and $-m_{\dot{\theta}}$ for the axis $x_0 = 0{\cdot}42\bar{c}$ have been evaluated from equations (11) and are plotted over the Mach number range $0{\cdot}7 \leqslant M \leqslant 1{\cdot}3$ in Figs. 5 to 8 respectively. The full curves for $\bar{\nu} \to 0$ indicate that the low-frequency theories give a fairly coherent picture for this range. Rapid variation is shown for $0{\cdot}9 \leqslant M \leqslant 1{\cdot}1$, particularly for the damping derivatives in Figs. 6 and 8; only $-m_{\dot{\theta}}$ is discontinuous at $M = 1$. Incomplete curves are shown for values of the frequency parameter $\bar{\nu} = 0{\cdot}3$ and 0·6. The results by Refs. 6 and 7 reveal the growing importance of frequency effects as M increases to high subsonic values. At $M = 1$, the derivatives for these frequencies by Ref. 11 are represented by shaded symbols; also plotted are the estimates of the derivatives and their rate of change near $M = 1$ by Ref. 10. These results for sonic flow correlate satisfactorily with both the subsonic and supersonic theories. When $M > 1$, the variation of the derivatives with M and $\bar{\nu}$ appears rather more complicated, but it is clearly seen that large frequency effects persist into the low supersonic range. The results by Ref. 19 provide a satisfactory link between the sonic results and those calculated for $M > 1{\cdot}2$ and $\bar{\nu} = 0{\cdot}3$ from the expansion in $\bar{\nu}$ in Ref. 14.

The corresponding low-frequency experimental results from Tables 5a, b and c are plotted in Figs. 5 to 8 over the respective Mach number ranges $0{\cdot}71 \leqslant M \leqslant 0{\cdot}87$ in the sealed 36 in. × 14 in. tunnel, $0{\cdot}84 \leqslant M \leqslant 1{\cdot}09$ in the slotted 36 in. × 14 in. tunnel and $1{\cdot}00 \leqslant M \leqslant 1{\cdot}18$ in the slotted 25 in. × 20 in. tunnel; the plotted data for the sealed tunnel correspond to the measurements corrected for wall interference. When $M \leqslant 0{\cdot}87$, low-frequency theory is in fairly good agreement with experiment except for the substantially lower experimental values of $l_{\dot{\theta}}$ in Fig. 6. For the derivatives $l_{\dot{\theta}}$, m_θ and $-m_{\dot{\theta}}$, experiment indicates a marked increase with subsonic M followed by a decrease through the sonic and supersonic speeds; this is broadly similar to the theoretical variation, but the region of most rapid change occurs experimentally at a lower Mach number as might be expected with a 10 per cent thick aerofoil section. On the other hand, in Fig. 5, there is a large reduction in the measured l_θ at $M = 0{\cdot}94$, 0·99 and 1·00, although the comparison between low-frequency theory and experiment improves at $M = 1{\cdot}10$ and 1·18. In Fig. 9, the theoretical m_θ and $-m_{\dot{\theta}}$ for $M = 0{\cdot}866$ and $\bar{\nu} \to 0$ are plotted against axis position x_0/c_r, together with the measured values for several axes given in Table 5d as

'$M = 0{\cdot}868$, Sealed 36 in. × 14 in. tunnel, Corrected'

and

'$M = 0{\cdot}844$, Slotted 36 in. × 14 in. tunnel, Uncorrected'.

Both sets of experiments give a variation of m_θ with axis position consistent with theory. The comparisons for $-m_{\dot{\theta}}$ are not so good, the measured results indicating less change with axis position than the theory

THIS DOCUMENT PROVIDED BY THE ABBOTT AEROSPACE
TECHNICAL LIBRARY
ABBOTTAEROSPACE.COM

predicts. A small theoretical effect of frequency on the pitching moment at $M = 0{\cdot}866$ is shown by the broken curves for $\bar{\nu} = 0{\cdot}3$ and $0{\cdot}6$.

The theoretical frequency effect is seen to be most marked near $M = 1$. By the analytical solution for $M = 1$ (Ref. 13), $-m_{\dot{\theta}}$ tends to infinity when $\bar{\nu} \to 0$, although the other pitching derivatives remain finite in Table 2c. For $0 \leqslant \bar{\nu} \leqslant 0{\cdot}6$ at $M = 1$, values of the derivatives l_θ and $l_{\dot{\theta}}$ for the axis $x_0 = 0{\cdot}42\bar{c}$ are plotted against $\bar{\nu}$ in Fig. 10. Results by the sonic theories in Chapters 4, 6, 7 of Ref. 10 are restricted to different ranges of $\bar{\nu}$ that are complementary, as indicated in Table 1. When $\bar{\nu} \to 0$, the results by Chapter 4 of Ref. 10 and by Ref. 13 are identical, whilst slender-wing theory gives the same stiffness derivatives but neglects terms of $0(A^2)$ in the damping derivatives. The full curves plotted in Fig. 10 represent the general collocation method of Ref. 11 applied with $m(N) = 13(3)$ terms; for $\bar{\nu} = 0{\cdot}2$, a solution $m(N) = 13(2)$ gives similar but less accurate results. Comparison of the various theories show that the method of Ref. 11 is in good agreement with the analytical solutions for $\bar{\nu} \geqslant 0{\cdot}2$; as expected, it deteriorates at smaller values of $\bar{\nu}$.

The variation of the direct pitching derivatives with axis position is illustrated in Figs. 11 to 13 for the transonic Mach numbers. For $M = 0{\cdot}99$ and $M = 1{\cdot}014$ in Figs. 11a and 11b respectively, $-m_{\dot{\theta}}$ is plotted against x_0/c_r for frequency parameters $\bar{\nu} \to 0$, $0{\cdot}3$ and $0{\cdot}6$. These theoretical results indicate a large decrease in pitching damping as the frequency increases, particularly for the supersonic Mach number. This characteristic is typical of the effect of much higher frequencies outside the transonic speed range. It is seen from Fig. 11 that the curves of $-m_{\dot{\theta}}$ for $\bar{\nu} = 0{\cdot}6$ are very similar at the two values of M. For Mach numbers in the range $0{\cdot}866 \leqslant M \leqslant 1{\cdot}2$, Figs. 12 and 13 respectively show curves of m_θ and $-m_{\dot{\theta}}$ for $\bar{\nu} = 0{\cdot}3$. Whilst m_θ shows relatively small changes with M, the curves of $-m_{\dot{\theta}}$ vary considerably. At all axis positions, $-m_{\dot{\theta}}$ increases rapidly as $M = 1$ is approached through subsonic or supersonic values. As M increases from $0{\cdot}866$ to $1{\cdot}2$, there is a progressive upstream shift in the position of minimum damping from $0{\cdot}65c_r$ to $0{\cdot}20c_r$; the derivative remains positive for all M in the range.

Linearized theory predicts the sonic and low-supersonic region as the most sensitive. This is illustrated in Figs. 14 and 15, by complete curves of m_θ and $-m_{\dot{\theta}}$ against M, by which the authors attempt to summarize the various theoretical and experimental data for the rectangular wing. Representative theoretical curves for $\bar{\nu} \to 0$, $0{\cdot}3$ and $0{\cdot}6$ are drawn for the wider range of Mach number $0{\cdot}4 \leqslant M \leqslant 1{\cdot}6$. In Fig. 14, the effect of frequency on m_θ is small when $M < 0{\cdot}8$ or $M > 1{\cdot}2$, but in the intermediate transonic range the derivative shows large variations with both Mach number and frequency. The rapid variation of the $\bar{\nu} \to 0$ curve just above $M = 1$ is a feature of the exact theoretical solution[13] and is retained; on the other hand, the numerical solutions for $\bar{\nu} = 0{\cdot}3$ and $0{\cdot}6$ have been smoothed on either side of $M = 1$ to give the curves in Fig. 14. The experimental data are limited to frequency parameters in the range $0{\cdot}07 < \bar{\nu} < 0{\cdot}16$, and the corresponding curve of m_θ agrees remarkably well with theory not only below $M = 0{\cdot}8$ but at the low supersonic speeds. The undulating experimental curve in the high subsonic range never departs far from the theoretical estimate. In Fig. 15, for reasons of clarity and lack of data, the $\bar{\nu} = 0{\cdot}6$ curve is not extended below $M = 0{\cdot}8$. The curve for $\bar{\nu} = 0{\cdot}3$ in this region makes use of the extension to subsonic low-frequency theory in equation (19) of Ref. 27, which becomes

$$(\partial m_{\dot{\theta}}/\partial \bar{\nu})_{\bar{\nu} \to 0} = (A/16)\,(l_\theta\, m_\theta)_{\bar{\nu} \to 0} \tag{13}$$

in the present notation. Fig. 15 shows small frequency effects for $M < 0{\cdot}8$ and also for $M > 1{\cdot}4$. The experimental curve shows fair agreement with theory outside the range $0{\cdot}9 < M < 1{\cdot}1$; within this transonic range it corresponds roughly to a theoretical curve for a frequency parameter between $0{\cdot}3$ and $0{\cdot}6$ displaced by $0{\cdot}05$ to $0{\cdot}10$ down the Mach number scale.

5. *Delta Wing* ($A = 1{\cdot}5$).

The variation of the pitching derivatives with Mach number, frequency and axis position is illustrated in Figs. 16 to 24 by subsonic, sonic and supersonic solutions taken from Tables 3a, b and c respectively. The results plotted for subsonic flow are the collocation solutions $m(N) = 11(3)$ by Refs. 4 and 7, $m(N) = 11(4)$ by Ref. 6 and $m(N) = 12(6)$ by Ref. 8. The collocation method of Ref. 11 with $m(N) = 14(3)$ is given

THIS DOCUMENT PROVIDED BY THE ABBOTT AEROSPACE
TECHNICAL LIBRARY
ABBOTTAEROSPACE.COM

for $M = 1$: some comparison with the analytical solutions for the delta wings from Refs. 9 and 10 is included. For low supersonic Mach numbers the expansion method of Ref. 15 is restricted to low frequency, but results from Ref. 19 cover the higher frequencies.

In Figs. 16 to 19, the pitching derivatives for the mid-root-chord axis $x_0 = \bar{c}$ are plotted against M for $0{\cdot}7 \leqslant M \leqslant 1{\cdot}3$. The full curves by Refs. 4 and 15 for $\bar{\nu} \to 0$ cover all but the high subsonic range $0{\cdot}99 < M < 1$. These subsonic and supersonic results in Figs. 16 and 18 indicate good correlation in l_θ near $M = 1$ but are rather less satisfactory for m_θ. The variation of these low-frequency derivatives with M is not large, especially when $M > 1$. On the other hand, in Figs. 17 and 19, the results for $l_{\dot{\theta}}$ and $-m_{\dot{\theta}}$ both tend to $+\infty$ or $-\infty$ as $M \to 1$ from below or above. It is therefore particularly interesting to study how the damping derivatives vary through the transonic region $0{\cdot}9 < M < 1{\cdot}1$ for the higher frequencies $\bar{\nu} = 0{\cdot}15$ and $0{\cdot}30$. Although $l_{\dot{\theta}}$ and $-m_{\dot{\theta}}$ decrease rapidly between $M = 0{\cdot}99$ and $M = 1{\cdot}03$, the values for the two finite frequencies are very similar. The frequency effects at higher Mach numbers diminish even more quickly than for the rectangular wing.

The effect of frequency on the sonic pitching-moment derivatives is illustrated in Fig. 20 for the axis $x_0 = 1{\cdot}5\bar{c}$. In the analytical solution for the derivative $-m_{\dot{\theta}}$ at small $\bar{\nu}$ (Ref. 9 or 15), the terms of $0(\log \bar{\nu})$ are found to cancel for this particular pitching axis, leading to a finite value for $-m_{\dot{\theta}}$ when $\bar{\nu} \to 0$. Furthermore, neglect of terms of $0(A^2)$ gives the slightly lower value for $-m_{\dot{\theta}}$ corresponding to slender-wing theory. For $\bar{\nu} \leqslant 0{\cdot}3$ in Fig. 20, the theories of Refs. 9 and 10 indicate a very small frequency effect on m_θ and $-m_{\dot{\theta}}$ for $x_0 = 1{\cdot}5\bar{c}$. The results by the collocation method of Ref. 11 are smaller in magnitude, but again show little effect of frequency when $\bar{\nu} > 0{\cdot}15$. At the lower frequencies, as for the rectangular wing in Fig. 10, the accuracy of the solutions $m(N) = 14(3)$ is seen to decrease, particularly for the damping derivative; moreover, the solution $m(N) = 14(2)$ gives poorer comparisons with the analytical results at $\bar{\nu} = 0{\cdot}05$.

Values of $-m_{\dot{\theta}}$ plotted against axis position x_0/c_r are presented in Figs. 21a and 21b for the Mach numbers $M = 0{\cdot}99$ and $M = 1{\cdot}01$. In Fig. 21a, the curves for $\bar{\nu} \to 0$, $0{\cdot}15$ and $0{\cdot}30$ show a steady decrease in $-m_{\dot{\theta}}$ as the frequency increases or as the axis moves downstream. On the supersonic side, however, the curves for $\bar{\nu} \to 0$ and $0{\cdot}15$ in Fig. 21b show an increase in $-m_{\dot{\theta}}$ with $\bar{\nu}$, although the curve for $\bar{\nu} = 0{\cdot}30$ indicates a subsequent decrease. For $\bar{\nu} = 0{\cdot}15$ and a wider range of Mach numbers, the variation of m_θ and $-m_{\dot{\theta}}$ with x_0/c_r is illustrated by Figs. 22 and 23 respectively. Over the range $0{\cdot}90 \leqslant M \leqslant 1{\cdot}281$, remarkably similar curves are obtained for each derivative as a function of x_0. There is a small increase in m_θ as the Mach number departs from unity for pitching axes forward of $x_0 = 0{\cdot}8c_r$. In Fig. 23, the curves of $-m_{\dot{\theta}}$ show less systematic changes with M, but the damping consistently decreases, whilst remaining positive, as the pitching axis moves downstream to $0{\cdot}8c_r$.

Measured values of $-m_{\dot{\theta}}$ are available from Ref. 26 for a complete delta wing of slightly lower aspect ratio $A = 1{\cdot}45$ with pitching axis $x_0 = 1{\cdot}2\bar{c}$. The summary of data in Fig. 24 corresponds to this axis and Mach numbers $0{\cdot}4 \leqslant M \leqslant 1{\cdot}6$. Theory and experiment compare satisfactorily throughout the subsonic speed range; close to $M = 1$ the experimental curve ($\bar{\nu} = 0{\cdot}13$) has similar shape to the theoretical curve for the frequency parameter $\bar{\nu} = 0{\cdot}15$. The estimated theoretical curve for $\bar{\nu} = 0{\cdot}30$ is omitted as it is virtually indistinguishable from that for $\bar{\nu} = 0{\cdot}15$. Since the pitching axis is near to the aerodynamic centre and m_θ is small, equation (13) gives a small value of $\partial m_{\dot{\theta}}/\partial \bar{\nu}$ in subsonic flow as $\bar{\nu} \to 0$. Only in the range $0{\cdot}9 < M < 1{\cdot}2$ is there appreciable frequency effect in Fig. 24. Marked disagreement in $-m_{\dot{\theta}}$ between experiment and theory appears as soon as the flow becomes supersonic. Similar differences are observed above $M = 1{\cdot}4$, and these may well continue up to $M = 2{\cdot}848$ when the leading edge becomes sonic.

6. *Symmetrical Tapered Wing* ($A = 4{\cdot}33$).

The various solutions for $M \leqslant 1$ and $M > 1$, given in Tables 4a and b respectively, are illustrated in Figs. 25 to 34 by the pitching derivatives as functions of Mach number or axis position when $\bar{\nu} \to 0$, $0{\cdot}19$ and $0{\cdot}38$. For this planform, the only analytical solutions available are the low-frequency results for $M \geqslant 1{\cdot}035$ by Ref. 16, and so greater emphasis is placed on the general numerical methods in supersonic flow. The subsonic collocation methods are represented by Refs. 4 and 7 with $m(N) = 11(3)$ and also by Refs. 6 and 8; the results plotted for $M = 1$ correspond to $m(N) = 14(3)$ by Ref. 11. In supersonic

THIS DOCUMENT PROVIDED BY THE ABBOTT AEROSPACE
TECHNICAL LIBRARY
ABBOTTAEROSPACE.COM

flow, the solutions are mainly from the box methods of Refs. 17 and 19, but Ref. 18 is represented by a collocation solution $m(N) = 10(4)$ at $M = 1{\cdot}102$.

The four derivatives l_θ, $l_{\dot\theta}$, m_θ and $-m_{\dot\theta}$ are plotted against Mach number in Figs. 25 to 28 for the mid-chord pitching axis $x_0 = 0{\cdot}79\bar{c}$. The full curves for the subsonic and supersonic theories when $\bar\nu \to 0$ show substantial changes in all these derivatives over the range $0{\cdot}9 \leqslant M \leqslant 1{\cdot}2$. Steady sonic theory gives $l_\theta = 3{\cdot}40$ and $m_\theta = 1{\cdot}37$; the corresponding damping derivatives at $M = 1$ are unknown, but they appear to include a singular contribution of $0(\log \bar\nu)$. The results for $\bar\nu = 0{\cdot}19$ and $0{\cdot}38$ indicate a very large frequency effect for the transonic Mach numbers, which persists into the supersonic range to a greater extent than for the other two planforms. The range of M is reasonably well covered for $\bar\nu = 0{\cdot}19$ with good correlation between the results by the different theories; for $\bar\nu = 0{\cdot}38$, however, there are greater uncertainties in the direct derivatives m_θ and $-m_{\dot\theta}$ for low supersonic M.

The measured pitching derivatives for $x_0 = 0{\cdot}79\bar{c}$ from Tables 6a to 6d provide experimental results for $\bar\nu < 0{\cdot}08$ over the whole Mach number range of Figs. 25 to 28. Here, the plotted data from Tables 6a and 6c for the two tunnels with slots or perforations sealed are the values corrected for wall interference. The variation with Mach number from these experiments ($M < 0{\cdot}87$) is similar to that predicted by theory, although the latter gives rather higher values of l_θ, $l_{\dot\theta}$, m_θ and $-m_{\dot\theta}$. For the slotted 36 in. $\times$ 14 in. tunnel and the perforated 25 in. $\times$ 20 in. tunnel, the values plotted from Tables 6b and 6d respectively cover the Mach numbers $0{\cdot}84 \leqslant M \leqslant 1{\cdot}09$ and $0{\cdot}85 \leqslant M \leqslant 1{\cdot}30$. Between these experimental results there are some quite large discrepancies, but neither set suggests such large variations near $M = 1$ as theory would indicate for $\bar\nu = 0{\cdot}05$. As already discussed in Section 3.2, these uncorrected transonic measurements could be subject to large, but uncertain, tunnel-wall interference. Figs. 25 to 28 show better agreement between theory and experiment for the supersonic values $M = 1{\cdot}2$ and $1{\cdot}3$, except perhaps in Fig. 26 where wall interference on $l_{\dot\theta}$ still predominates (Refs. 24). The variation of the subsonic pitching-moment derivatives with axis position and frequency parameter is illustrated in Fig. 29 by the values of m_θ and $-m_{\dot\theta}$ at $M = 0{\cdot}9$ plotted against x_0/c_r. Experimental results at four axis positions from Table 6e are in fairly good agreement with the theoretical curves of m_θ. For the damping derivative, however, the measurements (points Y) from the perforated 25 in. $\times$ 20 in. tunnel are consistently below theory, whilst those points X) from the slotted 36 in. $\times$ 14 in. tunnel indicate a larger rate of change of $-m_{\dot\theta}$ with x_0/c_r. The discrepancies between the two sets of experiments are attributed to the peculiar tunnel-wall interference effects mentioned in Section 3.2.

Theoretical values of $-m_{\dot\theta}$ at $M = 0{\cdot}99$ and $M = 1{\cdot}035$ are plotted against x_0/c_r in Figs. 30a and 30b respectively. For the subsonic case, the curves of $-m_{\dot\theta}$ for $\bar\nu \to 0$, $0{\cdot}063$, $0{\cdot}19$ and $0{\cdot}38$ show, as $\bar\nu$ increases, a large and progressive loss in the pitching damping for all axes. As the frequency increases in the supersonic case, there is a very large reduction in the rate of change of $-m_{\dot\theta}$ with x_0/c_r, until at $\bar\nu = 0{\cdot}38$ the two Mach numbers give similar curves of $-m_{\dot\theta}$. As for the rectangular wing in Fig. 11 at transonic speeds, these are typical high-frequency effects that appear to develop at surprisingly low frequencies. In Figs. 31 and 32, the pitching-moment derivatives for $\bar\nu = 0{\cdot}19$ are plotted against x_0/c_r for Mach numbers in the range $0{\cdot}90 \leqslant M \leqslant 1{\cdot}25$. Fig. 31 shows a very consistent variation in m_θ with x_0 for all M, and for a wide range of pitching axis there is a gradual decrease in this stiffness derivative as the Mach number grows. Fig. 32 illustrates the very large increase in damping as the axis position moves downstream or the Mach numbers approach $M = 1$ from above or below. Negative damping occurs at the forward axis positions for Mach numbers $1{\cdot}064 \leqslant M \leqslant 1{\cdot}25$, and this is typical of the higher aspect ratio of the symmetrical tapered wing.

The theoretical and experimental data in Figs. 27 and 28 are reproduced as estimated curves in Figs. 33 and 34 over the extended Mach number scale $0{\cdot}4 \leqslant M \leqslant 1{\cdot}6$. This allows additional supersonic experimental data from Ref. 25 to be included. The theoretical curves for non-zero frequency are known in detail above $M = 1{\cdot}1$ and are thought to be more reliable near $M = 1$ than for the other two wings. Additional results by Ref. 8 for $\bar\nu = 0{\cdot}63$ are used to extend the range of frequency on the subsonic side. In Fig. 33, faired theoretical curves of m_θ for the mid-chord axis are drawn; at the non-zero frequencies the derivative appears to have a minimum very near $M = 1$ and two maxima that spread away from $M = 1$ as $\bar\nu$ increases. As for the rectangular wing, the experimental curve fits the theoretical data satisfactorily at subsonic speeds; but, in contrast to Fig. 14, the curve is much flatter around $M = 1$. A rapid

THIS DOCUMENT PROVIDED BY THE ABBOTT AEROSPACE
TECHNICAL LIBRARY
ABBOTTAEROSPACE.COM

fall near $M = 1{\cdot}2$ leads to supersonic experimental data somewhat inconsistent with those of Ref. 25. As described in Ref. 16, allowance for the 5 per cent thick double-wedge aerofoil section gives the corrected low-frequency curve, added in Fig. 33, which lies between the two sets of experimental data. In Fig. 34, there is the familiar growth and decay of frequency effect on $-m_\theta$ through the transonic speed range, $0{\cdot}85 < M < 1{\cdot}30$ in this case. In the upper transonic range an increase in frequency eliminates negative damping for the mid-chord pitching axis. The mean experimental curve corresponds to frequency parameters $0{\cdot}03 < \bar{\nu} < 0{\cdot}08$ and is in excellent agreement with theory for the subsonic and supersonic ranges $M < 0{\cdot}9$ and $M > 1{\cdot}3$; for the latter, this is confirmed by the measurements of Ref. 25, in Fig. 8 of which a small theoretical correction for the double-wedge aerofoil improves the comparison of $-m_\theta$. Transonic flow appears to start abruptly at $M = 0{\cdot}9$ and results in an experimental curve similar in shape to a theoretical one for $\bar{\nu}$ just greater than $0{\cdot}2$ but with a positive displacement of $0{\cdot}10$ to $0{\cdot}15$ along the Mach number scale. It is interesting to note that this displacement is in the opposite sense to that observed for the rectangular wing in Fig. 15; the most likely explanation lies in the fact that the rectangular wing has a round-nosed section in contrast to the double-wedge section of the symmetrical tapered wing. If this is a true explanation, change to a round-nosed section might well introduce small or negative pitching damping on the symmetrical tapered wing at low frequencies in the transonic speed range, perhaps nearer to $M = 1$ than theory predicts.

7. *Appraisal of Theoretical Methods.*

In spite of the different characteristics of the three wings, it is possible to draw a few conclusions about the general theories that have been applied. Apart from the numerical results presented in Tables 2 to 4, there is extraneous evidence from less successful computations. The accuracy of collocation solutions in subsonic flow is also more clearly defined in the light of recent developments relating to Ref. 28. Contrasting features of the four subsonic theories of Table 1 have already been discussed in Section 2.1, and the appraisal is continued in Section 7.1. Likewise, the relative merits of Refs. 17 to 19 in supersonic flow are considered in Section 7.2 as a sequel to Section 2.3.

Ref. 11 is the only general theory for sonic flow discussed in Section 7.3, but we attempt to review the status of linearized theory in transonic flow. In this respect it is unfortunate that the experimental evidence is rather less conclusive than the composite theoretical analysis.

7.1. *Subsonic Flow.*

Subsequent to the present calculations for low frequency by the theory of Ref. 4, the improved programme of Ref. 28 has been developed. In Ref. 4, the parameter m as played a dual role in defining both the number of collocation sections and the number of spanwise integration points. It is now established that these should be independent, and in Ref. 28 the number of spanwise integration points is chosen to be

$$\bar{m} = q(m+1)-1\,, \tag{14}$$

where q is either unity or an even integer. It seems that collocation error in Ref. 4 is much less serious than spanwise integration error; in the present examples $m = 11$ is probably adequate, but $\bar{m}$ should be much greater. Moreover, the larger the number of chordwise terms (N), the larger q needs to be, since the integration errors are aggravated as collocation points approach the leading edge. With $N = 3$, changes in l_θ up to 3 per cent have been found as a result of increasing the parameter q, and there are corresponding errors in the other pitching derivatives. However, these would have smaller magnitude on Figs. 5 to 8, 16 to 19 or 25 to 28 than the worst subsonic discrepancies that appear. The largest errors can possibly be attributed to the use of larger values of N for which the parameter q is more crucial. The general criticism of Ref. 4 applies no less to Refs. 6 to 8 or indeed to any collocation method in which the chordwise integration of equation (1) is carried out first and insufficient attention is paid to the spanwise integration.

An exponential factor in the kernel function of Ref. 7 introduces a form of load distribution which, for damping terms in the limit as $\bar{\nu} \to 0$, becomes distinct from that in Ref. 4. However, Ref. 4 can easily be

THIS DOCUMENT PROVIDED BY THE ABBOTT AEROSPACE
TECHNICAL LIBRARY
ABBOTTAEROSPACE.COM

modified to be consistent with Ref. 7, and for the rectangular wing this has almost negligible effect on the damping derivatives. For practical purposes Refs. 4 and 7 may be regarded as equivalent in the limit as $\bar{\nu} \to 0$. A few comparisons between Refs. 4 and 8 are available for the rectangular wing ($M = 0{\cdot}8$, $\bar{\nu} = 0{\cdot}01$) in Table 2a and the delta wing ($M = 0{\cdot}80$ and $0{\cdot}99$, $\bar{\nu} = 0{\cdot}015$) in Table 3a; agreement is satisfactory, but less good in the latter case when a large number of chordwise terms ($N = 8$) is used. The comparisons between Refs. 4 and 6 for the rectangular ($M = 0{\cdot}99$, $\bar{\nu} = 0{\cdot}03$) and delta ($M = 0{\cdot}99$, $\bar{\nu} = 0{\cdot}015$) wings are rather poorer.

It is particularly unfortunate that the difficulty of spanwise integration so discredits Richardson's[6] method. Its distinctive feature is that N plays the dual role in numbering the chordwise collocation points and integration points. Computationally, this facilitates the extension to fairly large values of N; but the collocation points then extend so near the leading edge that errors in spanwise integration (with $q = 1$) seem prohibitive and result in wavy distributions of chordwise loading. In many applications the parameter N may inevitably be either too low for accurate chordwise integration of equation (1) or too high for accurate spanwise integration at every collocation point. The results for the rectangular and symmetrical tapered wings seem reasonably good, but the delta wing has proved the most difficult to handle by Ref. 6; the $m(N) = 10(6)$ solutions given in Ref. 20 for this wing have been largely ignored in favour of the 11(4) solutions. Yet the considerable frequency effect on $-m_{\dot{\theta}}$ between Refs. 4 and 6 in Fig. 19 is inconsistent in magnitude and sign with equation (13) of Section 4, unlike the point (O) at $M = 0{\cdot}9$ corresponding to Ref. 7. Indeed, the evidence from Ref. 6 has had to be ignored in the preparation of Fig. 24.

The only direct comparison between Refs. 7 and 8, for the rectangular wing with $M = 0{\cdot}99$ and $\bar{\nu} = 0{\cdot}6$, is quite encouraging, and other results by the two theories appear to be reasonably consistent. No conclusions are possible regarding the relative merit of odd or even values of m (Section 2.1). Both methods suffer from the computational difficulties that are now imposed by the need for a large number of spanwise integration points, but less so than Ref. 6. Given a large enough computer, a desirable improvement in each method would result from increasing the number from m to $\bar{m}$ by a technique similar to that used in Ref. 28 with equation (14). Without this refinement, however, the direct pitching derivatives m_θ (Figs. 14, 33) and $-m_{\dot{\theta}}$ (Figs. 15, 24, 34) show a broad pattern of good correlation between theory and experiment for the three wings over the range of Mach number $M \leqslant 0{\cdot}85$. In this sub-critical range, with the possible exception of $l_{\dot{\theta}}$, the measured derivatives depart from linearized theoretical prediction by amounts that are quite compatible with likely effects of aerofoil thickness or viscosity.

7.2. *Supersonic Flow.*

For each of the wings in supersonic flow the results of linearized theory can be obtained with confidence, provided that the Mach number is high enough and the frequency small enough, say, $M > 1{\cdot}2$ and $\bar{\nu} < 0{\cdot}2$. Consider first the manner in which exact special theories give place to approximate general theories as the Mach number decreases and the frequency parameter remains constant. For the rectangular wing in Figs. 5 to 8, the link between Refs. 14 and 19 looks satisfactory for all four derivatives when $\bar{\nu} = 0{\cdot}3$. Likewise for the delta wing at $\bar{\nu} = 0{\cdot}15$ in Figs. 16 to 19, there is fairly convincing agreement between Refs. 15 and 19, the worst difference being of order 0·05 in $l_{\dot{\theta}}$. For the symmetrical tapered wing at $\bar{\nu} = 0{\cdot}19$, the lift derivatives in Figs. 25 and 26 follow smoothly enough from Ref. 17 to Ref. 19, but discrepancies of about 0·1 in m_θ and 0·5 in $-m_{\dot{\theta}}$ appear in Figs. 27 and 28.

Since two of the wings have streamwise symmetry, it is interesting to apply the reverse-flow theorem to obtain exact relationships between the derivatives, as in equations (41) of Ref. 29. With the aid of equations (11) and (12) and with representative length $\bar{c}$, it is found that the coefficients $A,B,\ldots H$ should satisfy the identities

$$F + (c_r/\bar{c})\, B + D \equiv 0 \tag{15}$$

and

$$H + (c_r/\bar{c})\, D - B/\bar{\nu}^2 \equiv 0\,. \tag{16}$$

From the results in Tables 2c and 4b, excluding cases in which $\bar{\nu} \leqslant 0{\cdot}1$, the following table of typical magnitudes of the left-hand sides of equations (15) and (16) is obtained.

THIS DOCUMENT PROVIDED BY THE ABBOTT AEROSPACE
TECHNICAL LIBRARY
ABBOTTAEROSPACE.COM

Wing	Method	Typical magnitude	
		Equation (15)	Equation (16)
Rectangular	Ref. 19	$0{\cdot}00_5$	$0{\cdot}01_5$
Symmetrical tapered	Ref. 17	0·00	$0{\cdot}01_5$
	Ref. 18	0·00	0·02
	Ref. 19	0·01	0·07

With the possible exception of the value 0·07 from equation (16) by Ref. 19, the listed discrepancies are negligible in the present context. Equations (15) and (16) can never give positive assurance of accuracy; the derivatives m_θ and $-m_{\dot{\theta}}$, which are most in doubt for the symmetrical tapered wing, involve the coefficients E and G that do not appear in these equations. The particular values of E and G in Table 4b for $M = 1{\cdot}102$ and $\bar{\nu} = 0{\cdot}19$ show Refs. 18 and 19 in fair agreement and cast some doubt on results of Ref. 17 for $M = 1{\cdot}105$ and $\bar{\nu} = 0{\cdot}19$. Rightly or wrongly, Ref. 17 is given full credit in Figs. 33 and 34, because of its convincing behaviour relative to the exact theoretical curves in the limit $\bar{\nu} \to 0$.

In view of the large frequency effects and rapid variations with Mach number in Figs. 25 to 28, the results at $M = 1{\cdot}102$ for two frequencies by the method of Harris[18] are fairly encouraging. But those for the delta wing by Ref. 18 in Table 3c would plot rather unsatisfactorily on Figs. 16 to 19. Now, a fairly slender delta wing at a low supersonic Mach number presents a severe challenge to a collocation method; in view of the small number of collocation points, examination of the solutions in Table 3c shows that the method has promise. Moreover, in the calculations of Ref. 30 for another series of planforms at higher Mach numbers, Ref. 18 appears to achieve success; further theoretical comparisons in Ref. 31 confirm this.

The most important general supersonic theory in the present investigation is Ref. 19, developed specially by Allen and Sadler and programmed for the Pegasus computer. This is a highly complex box method in which refinements abound. Not only is there careful treatment of incomplete boxes, shaded in Fig. 4, but for the delta wing at low supersonic Mach numbers there is a supplementary procedure to improve accuracy in surface integration when the ratio of box span to local wing span is no longer small. The theory caters for subsonic and supersonic leading and trailing edges and has been applied to each of the three wings at or near $M = 1{\cdot}01$. The solution for the rectangular wing at $M = 1{\cdot}05$ and $\bar{\nu} = 0{\cdot}3$ in Figs. 5 and 7 appears unsatisfactory, and those for the symmetrical tapered wing at $M = 1{\cdot}035$ and $M = 1{\cdot}064$ in Figs. 25 to 28 are hard to reconcile. The reverse-flow check from equation (16) for Ref. 19 is not perfect. In spite of these minor criticisms the theory ranks as a considerable achievement. Unfortunately, the programme of calculation is exceedingly complicated, and for a small computer this has proved a serious drawback. In a later research contract to obtain additional results for the delta wing, the supplementary procedure failed to operate and the calculations without it were unsuccessful; for some other reason the Pegasus computer programme failed in the tip region of the symmetrical tapered planform. As mentioned at the end of Section 3.1, the error was confirmed by a special application of Ref. 17, and for $M = 1{\cdot}08$ and $\bar{\nu} = 0{\cdot}19$ the DEUCE programme was used to correct faulty values of the velocity potential. The solution in Table 4b was then completed by the Pegasus programme and used satisfactorily in Figs. 25 to 28. That a simpler, more restrictive, programme should come to the rescue of a highly refined one illustrates the danger of over-elaboration. Correctly applied by its authors, Ref. 19 has made the present investigation possible and has enabled the continuous curves of Figs. 14, 15, 24, 33 and 34 for non-zero frequency to be drawn in the speed range $1{\cdot}0 < M < 1{\cdot}1$.

A final comment on supersonic theory follows from Fig. 2. The Mach lines illustrate the complexity of the problems for the rectangular and symmetrical tapered planforms. Each distinct region, bounded

THIS DOCUMENT PROVIDED BY THE ABBOTT AEROSPACE
TECHNICAL LIBRARY
ABBOTTAEROSPACE.COM

by reflected Mach lines from the wing tips, usually implies discontinuous curvature in the derivatives against M at the critical value where the particular region first appears on the planform. The delta wing, on the other hand, is free from such effects; yet its slenderness and its subsonic leading edge have made it the most difficult of the three planforms to treat by general methods. It may be asked, how profitable a similar investigation for other types of planform would be. Present experience for the delta wing tends to discourage the study of a slender wing with curved edges. A tapered wing with sweptback trailing edge is, perhaps, more promising, but there is no counterpart to the particular exact theories on which the present investigation leans so heavily. As for the delta wing in Fig. 24, serious discrepancies between linearized theory and experiment might well extend far into the supersonic speed range until both leading and trailing edges have become supersonic.

7.3. *Transonic Flow.*

The only general theory considered for $M = 1$ is that of Davies[11], and the results in Figs. 10, 20, 31 and 32 show an encouraging measure of success for each of the three planforms. In Table 2b for the rectangular wing with $\bar{\nu} = 0{\cdot}20$, there appears to be excellent convergence as the number of chordwise terms (N) is increased from 2 to 4. There are indications for the rectangular and delta wings in Figs. 10 and 20 that an increase in N improves comparisons between Ref. 11 and analytical theory. The corresponding convergence for the symmetrical tapered wing with $\bar{\nu} = 0{\cdot}38$ in Table 4a is less impressive, but remains satisfactory. All in all, the theory provides a confident link between those for subsonic and supersonic flow, unless $\bar{\nu}$ falls below 0·1, say. With this limitation Ref. 11 can be expected to apply to a wide range of planform.

The present investigation has revealed two interpretations of transonic flow. From the linearized theoretical standpoint it may be regarded as a narrow region in which the effects of frequency and Mach number become very large. On this rough basis the graphical results lead to the following table of ranges.

Wing	A	Transonic range
Rectangular	2·00	$0{\cdot}95 < M < 1{\cdot}15$
Delta	1·50	$0{\cdot}97 < M < 1{\cdot}05$
Symmetrical tapered	4·33	$0{\cdot}90 < M < 1{\cdot}20$

Having regard to Ref. 27 and equation (13), we might expect that the extent below $M = 1$ would increase with aspect ratio. The same tends to be true above $M = 1$, but it is remarkable how rapidly the theoretical transonic disturbances on the delta wing disappear. From the practical standpoint, however, non-linear effects of wing thickness, shock waves and boundary layers must lead to a broader interpretation of transonic flow. All wings are expected to show discrepancies between theory and experiment in the range $0{\cdot}9 < M < 1{\cdot}2$; there is evidence at higher Mach numbers from Ref. 31, as well as Fig. 24, that the discrepancies persist for wings with subsonic leading edges.

This leads us to consider the status of linearized theory in the transonic speed range. Given fairly reliable theoretical curves, it is pertinent to discuss how these illuminate or are illuminated by the experimental data. Figs. 14 and 33 suggest that, although theory predicts the order of magnitude of m_θ, empirical improvements would be difficult. By contrast, there is a tendency for the experimental curves of pitching damping in the high subsonic or low supersonic region to adopt shapes that resemble theoretical curves with the frequency parameter more than doubled; moreover, such comparative curves may need to be displaced one way or the other along the Mach number scale (Figs. 15, 24 and 34). It would be difficult to assess the purely theoretical shortcomings due to linearization, but these are probably large in the transonic region and could conceivably account for the types of discrepancy mentioned above. On the other hand, the experimental data are bedevilled by uncertainties of wall interference, which preclude further appraisal of transonic theoretical results.

THIS DOCUMENT PROVIDED BY THE ABBOTT AEROSPACE
TECHNICAL LIBRARY
ABBOTTAEROSPACE.COM

The present difficulties of wall interference on the damping derivatives are threefold. As explained in Section 3.2, both the slotted 36 in. × 14 in. and perforated 25 in. × 20 in. tunnels had uncertain wall conditions outside the transonic range, but the interference problem goes deeper than this. Even for other ventilated tunnels to which Ref. 23 can be applied in subsonic flow, large interference persists at transonic speeds when there is no theory of wall correction. Furthermore, it is demonstrated in Ref. 24, that interference-free conditions cannot readily be extrapolated from experimental results on smaller and smaller half-models, because of the dominant influence of the tunnel-wall boundary layer. If this were removed or thinned, the delta wing could usefully be tested as a half-model and an extended programme of dynamic measurements on the other two wings would clearly be desirable. Firmer conclusions might then be drawn from the combined theoretical and experimental analysis.

8. *Conclusions.*

(1) Linearized subsonic, sonic and supersonic theories give results that can be linked approximately by continuous curves of pitching derivatives for fixed values of the frequency parameter.

(2) The delta wing is more difficult to treat by general theories than the rectangular or symmetrical tapered wing, but in each case exact supersonic theory has provided a vital source of confidence.

(3) Although the same general theories could be applied to many other types of wing, a similar investigation for a slender curved planform would be rather difficult, but a sweptback tapered wing would be more promising.

(4) From a theoretical standpoint the transonic speed range may be defined as a limited region in which effects of frequency and Mach number become very large. This range appears to broaden with increasing aspect ratio and to narrow with increasing sweepback.

(5) For the unswept wings near $M = 1$, the theoretical damping derivatives show marked decreases in magnitude and less dependence on Mach number as the frequency parameter increases. These are typical high-frequency effects that develop surprisingly quickly with frequency at transonic speeds.

(6) The available comparisons between theory and experiment are satisfactory in purely subsonic or supersonic flow, with the reservations that the measured lift damping derivative $l_{\dot{\theta}}$ is somewhat below theory in subsonic flow and that for swept wings the practical transonic speed range may extend until the leading edge is supersonic.

(7) Curves of experimental damping derivatives against Mach number near $M = 1$ tend to resemble the theoretical curves with the frequency parameter more than doubled and with a positive or negative shift in Mach number, possibly dependent on aerofoil section.

(8) It is essential to devise interference-free experiments at transonic speeds, particularly on the damping derivatives. This should lead to more precise inference from combined theoretical and experimental analysis.

(9) If the present investigation were extended thus, it would stand as a yard-stick for the appraisal of any subsequent non-linear approaches to the formidable problem of transonic lifting-surface theory.

9. *Acknowledgements.*

The authors with to acknowledge helpful discussions with Mr. W. E. A. Acum of the Ship Division, NPL, and with Mr. D. L. Woodcock of the Structures Department of the Royal Aircraft Establishment. The work of Refs. 19 and 20 and subsequent calculations by the method of Ref. 19 were carried out under separate external contracts sponsored by the Ministry of Aviation. Sources of published and unpublished theoretical data are given in Section 3.1. Nearly all the remaining calculations were carried out by Mrs. S. Lucas of the Aerodynamics Division, NPL. Mr. K. C. Wight, also of the Aerodynamics Division, supplied the unpublished NPL experimental data.

THIS DOCUMENT PROVIDED BY THE ABBOTT AEROSPACE
TECHNICAL LIBRARY
ABBOTTAEROSPACE.COM

LIST OF SYMBOLS

A	Aspect ratio of planform
$A,B \ldots H$	Coefficients in equations (11) and (12)
$c(y)$	Local chord of wing
$\bar{c}$	Geometric mean chord, $S/2s$
c_r	Root chord of wing
h	Non-dimensional pitching axis, $x_0/\bar{c}$
K	Kernel function in equation (1)
$l(x,y)$	Non-dimensional wing loading
$l_z,l_{\dot{z}}$	Lift derivatives in equations (12) for plunging motion
$l_\theta,l_{\dot{\theta}}$	Lift derivatives in equations (11) for pitching motion
L	Lift force on wing
m	Number of collocation stations across wing span
$\bar{m}$	Number of integration stations across wing span
$m_z,m_{\dot{z}}$	Moment derivatives in equations (12) for plunging motion
$m_\theta,m_{\dot{\theta}}$	Moment derivatives in equations (11) for pitching motion
M	Mach number of free stream
$\mathscr{M}$	Nose-up pitching moment on wing
N	Number of collocation points along the chord
p	Integer or subscript in equation (2) defining chordwise collocation point
q	Integer in equation (14) relating m and $\bar{m}$
s	Semi-span of wing
S	Area of planform
t	Time
U	Velocity of free stream
w	Upward component of velocity
x,y,z	Rectangular co-ordinates in Fig. 3
x_0	Distance of pitching axis downstream of root leading edge
$x_l(y)$	Leading edge of wing referred to root
z_0	Amplitude of plunging oscillation as a fraction of $\bar{c}$
β	Supersonic compressibility factor, $(M^2-1)^{\frac{1}{2}}$
θ_0	Amplitude of oscillatory pitching motion
Λ_L	Angle of sweepback of leading edge
ν	Integer or subscript in equation (3) defining spanwise collocation station
$\bar{\nu}$	Frequency parameter, $\omega\bar{c}/U$
ρ	Density of free stream
ω	Circular frequency of oscillation

THIS DOCUMENT PROVIDED BY THE ABBOTT AEROSPACE
TECHNICAL LIBRARY
ABBOTTAEROSPACE.COM

REFERENCES

No.	*Author(s)*	*Title, etc.*
1	W. E. A. Acum and H. C. Garner	The estimation of oscillatory wing and control derivatives. A.R.C. C.P.623. AGARD Report 340. 1961.
2	W. E. A. Acum	The comparison of theory and experiment for oscillating wings. *Manual on Aeroelasticity*, Vol. 2, Ch. 10. AGARD (ed., W. P. Jones). A.R.C. C.P.681. 1962.
3	D. E. Williams	Three-dimensional subsonic theory. *Manual on Aeroelasticity*, Vol. 2, Ch. 3. AGARD (ed., W. P. Jones). A.R.C. R. & M. 3302. 1961.
4	H. C. Garner	Multhopp's subsonic lifting-surface theory of wings in slow pitching oscillations. A.R.C. R. & M. 2885. 1952.
5	C. E. Watkins, H. L. Runyan and D. S. Woolston	On the kernel function of the integral equation relating lift and downwash distributions of oscillating finite wings in subsonic flow. N.A.C.A. Report 1234. 1955.
6	J. R. Richardson	A method for calculating the lifting forces on wings (Unsteady subsonic and supersonic lifting-surface theory). A.R.C. R. & M. 3157. 1955.
7	W. E. A. Acum	Theory of lifting surfaces oscillating at general frequencies in a subsonic stream. A.R.C. R. & M. 3557. 1959.
8	D. E. Davies	Calculation of unsteady generalised airforces on a thin wing oscillating harmonically in subsonic flow. A.R.C. R. & M. 3409. 1963.
9	K. W. Mangler	A method of calculating the short-period longitudinal stability derivatives of a wing in linearised unsteady compressible flow. A.R.C. R. & M. 2924. 1952.
10	M. T. Landahl	*Unsteady Transonic Flow Theory.* Pergamon Press. 1961.
11	D. E. Davies	Three-dimensional sonic theory. *Manual on Aeroelasticity*, Vol. 2, Ch. 4. AGARD (ed., W. P. Jones).
12	C. E. Watkins	Three-dimensional supersonic theory. *Manual on Aeroelasticity*, Vol. 2, Ch. 5. AGARD (ed., W. P. Jones).
13	J. W. Miles	On the low aspect ratio oscillating wing in supersonic flow. *Aeronaut. Quart.* Vol. IV, p. 231. 1953.
14	H. C. Nelson, R. A. Rainey and C. E. Watkins	Lift and moment coefficients expanded to the seventh power of the frequency for oscillating rectangular wings in supersonic flow and applied to a specific flutter problem. NACA TN–3076. 1954.
15	D. E. Davies	The velocity potential on triangular and related wings with subsonic leading edges oscillating harmonically in supersonic flow. A.R.C. R. & M. 3229. 1959.

THIS DOCUMENT PROVIDED BY THE ABBOTT AEROSPACE
TECHNICAL LIBRARY
ABBOTTAEROSPACE.COM

REFERENCES—*continued*

No.	*Author(s)*	*Title, etc.*
16	D. E. Lehrian	Calculation of stability derivatives for tapered wings of hexagonal planform oscillating in a supersonic stream. A.R.C. R. & M. 3298. 1960.
17	K. Stewartson	On the linearized potential theory of unsteady supersonic motion. Part II. *Q. Jl. Mech. appl. Math.* Vol. 5, p. 137. 1952.
18	G. Z. Harris	The calculation of generalised forces on oscillating wings in supersonic flow by lifting surface theory. A.R.C. R. & M. 3453. 1965.
19	D. J. Allen and D. S. Sadler	Oscillatory aerodynamic forces in linearised supersonic flow for arbitrary frequencies, planforms and Mach numbers. A.R.C. R. & M. 3415. 1963.
20	G. E. G. Bishop	Flutter derivatives in the transonic range. de Havilland Aircraft Company. D. H. Aero Dept./2942/GEGB/GEN. 1961.
21	D. L. Woodcock	On the accuracy of collocation solutions of the integral equation of linearised subsonic flow past an oscillating aerofoil. *Proceedings of the International Symposium on Analogue and Digital Techniques Applied to Aeronautics*, Liège, 9th–12th September, 1963.
22	H. C. Garner, W. E. A. Acum and D. E. Lehrian	Comparative calculations of supersonic pitching derivatives over a range of frequency parameter. A.R.C. C.P.591. 1961.
23	H. C. Garner, A. W. Moore and K. C. Wight ..	The theory of interference effects on dynamic measurements in slotted-wall tunnels at subsonic speeds and comparisons with experiment. A.R.C. R. & M. 3500. 1966.
24	A. W. Moore and K. C. Wight	An experimental investigation of wall interference effects on dynamic measurements on half models in ventilated tunnels through the transonic speed range. A.R.C. R. & M. 3570. 1967.
25	L. Woodgate, J. F. M. Maybrey and C. Scruton	Measurements of the pitching-moment derivatives for rigid tapered wings of hexagonal planform oscillating in supersonic flow. A.R.C. R. & M. 3294. 1961.
26	K. Orlik-Rückemann and C. O. Olsson ..	A method for the determination of the damping-in-pitch of semi-span models in high-speed wind-tunnels, and some results for a triangular wing. F.F.A. Report 62. 1956.
27	H. C. Garner and R. D. Milne	Asymptotic expansion for transient forces from quasi-steady subsonic wing theory. *Aeronaut. Quart.*, Vol. XVII, pp. 343-350. 1966.
28	H. C. Garner and D. A. Fox ..	ALGOL 60 programme for Multhopp's low-frequency subsonic lifting-surface theory. A.R.C. R. & M. 3517. 1966.

THIS DOCUMENT PROVIDED BY THE ABBOTT AEROSPACE
TECHNICAL LIBRARY
ABBOTTAEROSPACE.COM

REFERENCES—*continued*

No.	*Author(s)*	*Title, etc.*
29	D. E. Lehrian and H. C. Garner	Comparative numerical applications of the reverse-flow theorem to oscillating wings and control surfaces. A.R.C. R. & M. 3488. 1965.
30	G. Z. Harris	Supersonic flutter derivatives for a series of swept and cropped delta wings. A.R.C. C.P.920. 1966.
31	D. L. Woodcock	Co-ordinated experimental and theoretical research on the oscillatory airforces for selected planforms at subsonic and supersonic speeds. A.R.C. R. & M. 3581. 1968.

TABLE 1

Theoretical Methods used to obtain Numerical Results.

Method	Author(s)	Description	Range of applicability			Results
			M	$\bar{\nu}$	Planform	
Ref. 4	Garner	Collocation	< 1	$\rightarrow 0$	General	—
Ref. 6	Richardson	Collocation	< 1	Any	General	Ref. 20
Ref. 7	Acum	Collocation	< 1	Any	General	—
Ref. 8	Davies	Collocation	< 1	Any	General	Ref. 21
Ref. 9	Mangler	Analytical	1	$< \frac{1}{4}A^{-2}$	Delta	Ref. 9
Ref. 10	Landahl	Expansion in $\bar{\nu}$	1	$< A^{-2}$	Delta	Chap. 3
Rer. 10	Landahl	Expansion in $\bar{\nu}$	1	$< A^{-2}$	Rectangular	Chap. 4
Ref. 10	Landahl	Analytical	1	$> 2A^{-2}$	Rectangular	Chap. 6
Ref. 10	Landahl	Analytical	1	$\geqslant A^{-2}$	Rectangular	Chap. 7
Ref. 11	Davies	Collocation	1	Not small	General	—
Ref. 13	Miles	Analytical	$\geqslant 1$	$\rightarrow 0$	Rect., $\beta A < 1$	Ref. 13
Ref. 14	Nelson *et al*	Expansion in $\bar{\nu}$	> 1	Not large	Rect., $\beta A \geqslant 1$	Ref. 14
Ref. 15	Davies	Expansion in $\bar{\nu}$	> 1	Small	Delta, $\beta A \leqslant 4$	—
Ref. 16	Lehrian	Analytical	> 1	$\rightarrow 0$	$\beta \geqslant \tan \Lambda_L$	Ref. 16
Ref. 17	Stewartson	Numerical	> 1	Any	$\beta \geqslant \tan \Lambda_L$	Ref. 22
Ref. 18	Harris	Collocation	> 1	Any	General	Ref. 18
Ref. 19	Allen and Sadler	Numerical	> 1	Any	General	Ref. 19

THIS DOCUMENT PROVIDED BY THE ABBOTT AEROSPACE
TECHNICAL LIBRARY
ABBOTTAEROSPACE.COM

TABLE 2a

Theoretical Derivatives for the Rectangular Wing ($A = 2$) in Subsonic Flow.

Method				l_θ	l_z	$l_{\dot\theta}$	$l_{\dot z}$	$-m_\theta$	$m_z - l_\theta$	$-m_{\dot\theta}$	$m_{\dot z} - l_{\dot\theta}$
Ref.	$m(N)$			A	B	C	D	E	F	G	H
4	7(3)	0·866	→0	1·462	0	1·633	1·462	0·242	−1·462	1·060	−1·875
	11(3)	0·600	→0	1·327	0	1·428	1·327	0·260	−1·327	0·739	−1·688
		0·800		1·417	0	1·548	1·417	0·254	−1·417	0·922	−1·803
		0·866		1·461	0	1·633	1·461	0·244	−1·461	1·060	−1·876
		0·925		1·508	0	1·777	1·508	0·220	−1·508	1·299	−1·997
		0·950		1·531	0	1·892	1·531	0·199	−1·531	1·486	−2·090
		0·970		1·549	0	2·043	1·549	0·171	−1·549	1·731	−2·214
		0·990		1·567	0	2·388	1·567	0·118	−1·567	2·278	−2·506
6	8(8)	0·990	0·03	1·567	−0·001	2·297	1·566	0·114	−1·566	2·174	−2·412
	8(8)	0·970	0·10	1·563	−0·006	2·009	1·558	0·178	−1·552	1·722	−2·192
		0·990		1·593	−0·008	2·294	1·586	0·129	−1·577	2·279	−2·427
	8(8)	0·866	0·30	1·474	−0·038	1·612	1·464	0·249	−1·426	1·042	−1·882
		0·900		1·524	−0·040	1·677	1·508	0·246	−1·468	1·177	−1·946
		0·925		1·574	−0·042	1·739	1·549	0·245	−1·508	1·329	−2·009
		0·950		1·643	−0·044	1·808	1·605	0·258	−1·562	1·565	−2·088
		0·970		1·721	−0·044	1·840	1·667	0·300	−1·623	1·816	−2·149
		0·990		1·800	−0·039	1·783	1·730	0·389	−1·691	1·971	−2·155
	8(6)	0·990	0·30	1·762	−0·042	1·810	1·703	0·367	−1·661	1·851	−2·161
	10(6)	0·990		1·754	−0·043	1·819	1·696	0·362	−1·655	1·832	−2·166
	8(8)	0·900	0·60	1·723	−0·127	1·575	1·630	0·349	−1·503	1·260	−1·976
		0·950		1·895	−0·055	1·341	1·731	0·561	−1·677	1·316	−1·877
		0·990		1·956	−0·051	1·359	1·791	0·616	−1·742	1·295	−1·930

THIS DOCUMENT PROVIDED BY THE ABBOTT AEROSPACE
TECHNICAL LIBRARY
ABBOTTAEROSPACE.COM

TABLE 2a—*continued*

Method		M	$\bar{v}$	l_θ	l_z	$l_{\dot\theta}$	$l_{\dot z}$	$-m_\theta$	$m_z - l_\theta$	$-m_{\dot\theta}$	$m_{\dot z} - l_{\dot\theta}$
Ref.	$m(N)$			A	B	C	D	E	F	G	H
7	7(3)	0·866	0·30	1·486	−0·043	1·692	1·478	0·235	−1·435	1·101	−1·950
			0·60	1·625	−0·167	1·699	1·577	0·264	−1·413	1·193	−2·038
	11(3)	0·866	0·30	1·486	−0·043	1·691	1·477	0·237	−1·434	1·102	−1·951
	11(3)	0·990	0·10	1·592	−0·009	2·310	1·584	0·124	−1·576	2·318	−2·438
			0·30	1·856	−0·037	1·784	1·772	0·418	−1·738	2·118	−2·182
			0·60	1·982	+0·034	1·022	1·772	0·738	−1·809	1·167	−1·665
8	20(2)	0·800	0·01	1·414	0·000	1·542	1·414	0·258	−1·414	0·915	−1·800
		0·800	1·00	1·516	−0·454	1·622	1·554	0·218	−1·103	0·940	−2·010
		0·990	1·00	1·997	−0·022	1·096	1·709	0·632	−1·689	0·931	−1·715
	20(4)	0·800	0·01	1·417	0·000	1·550	1·417	0·254	−1·417	0·922	−1·804
		0·800	1·00	1·661	−0·471	1·666	1·633	0·249	−1·176	1·100	−2·090
		0·990	1·00	1·960	+0·059	0·915	1·669	0·810	−1·731	0·833	−1·604
	12(6)	0·990	0·60	1·990	0·024	1·076	1·782	0·725	−1·808	1·207	−1·717
			1·00	1·953	0·055	0·917	1·665	0·815	−1·724	0·836	−1·608

THIS DOCUMENT PROVIDED BY THE ABBOTT AEROSPACE
TECHNICAL LIBRARY
ABBOTTAEROSPACE.COM

TABLE 2b

Theoretical Derivatives for the Rectangular Wing ($A = 2$) in Transonic Flow.

Method		M	$\bar{v}$	l_θ	l_z	$l_{\dot\theta}$	$l_{\dot z}$	$-m_\theta$	$m_z - l_\theta$	$-m_{\dot\theta}$	$m_{\dot z} - l_{\dot\theta}$
Ref.	$m(N)$			A	B	C	D	E	F	G	H
10	Chap. 7	0·9	0·30	1·895	−0·071	2·110	1·837	0·413	−1·573	2·360	−2·505
			0·60	2·079	−0·033	1·308	1·691	0·736	−1·649	1·367	−1·962
	Chap. 4	1·0	0·03	1·577	−0·001	2·693	1·575	0·021	−1·574	3·716	−2·714
			0·10	1·621	−0·011	2·566	1·608	0·084	−1·597	3·202	−2·652
			0·20	1·745	−0·035	2·320	1·704	0·211	−1·665	2·797	−2·536
	Chap. 7	1·0	0·25	1·86	−0·03	2·02	1·78	0·40	−1·76	2·45	−2·40
			0·30	1·93	−0·02	1·77	1·81	0·50	−1·81	2·11	−2·23
			0·50	1·99	+0·03	1·11	1·80	0·70	−1·83	1·35	−1·73
	Chap. 6	1·0	0·60	1·982	0·065	0·933	1·765	0·750	−1·830	1·103	−1·584
11	13(3)	1·0	0·03	1·631	0·001	0·912	1·630	0·091	−1·630	1·505	−1·004
			0·10	1·596	−0·008	2·321	1·586	0·066	−1·576	2·862	−2·388
			0·20	1·753	−0·033	2·308	1·710	0·262	−1·672	2·866	−2·563
			0·30	1·904	−0·034	1·776	1·815	0·479	−1·776	2·252	−2·228
			0·60	2·015	+0·042	1·035	1·797	0·768	−1·843	1·191	−1·707
	13(2)	1·0	0·20	1·812	−0·038	2·438	1·763	0·336	−1·725	2·998	−2·760
	13(4)	1·0	0·20	1·760	−0·031	2·267	1·717	0·273	−1·681	2·822	−2·533
	9(4)	1·0	0·20	1·768	−0·031	2·265	1·722	0·278	−1·688	2·846	−2·535

THIS DOCUMENT PROVIDED BY THE ABBOTT AEROSPACE
TECHNICAL LIBRARY
ABBOTTAEROSPACE.COM

TABLE 2c

Theoretical Derivatives for the Rectangular Wing ($A = 2$) in Supersonic Flow.

Method		M	$\bar{\nu}$	l_θ	l_z	$l_{\dot\theta}$	$l_{\dot z}$	$-m_\theta$	$m_z - l_\theta$	$-m_{\dot\theta}$	$m_{\dot z} - l_{\dot\theta}$
Ref.	$m(N)$			A	B	C	D	E	F	G	H
13	—	1·000	→0	1·571	0	2·749	1·571	0	−1·571	∞	−2·749
		1·005		1·574	0	2·480	1·574	0·006	−1·574	4·109	−2·486
		1·010		1·582	0	2·103	1·582	0·020	−1·582	3·424	−2·123
		1·014		1·556	0	3·279	1·556	−0·004	−1·556	4·566	−3·275
		1·020		1·528	0	4·075	1·528	−0·037	−1·528	5·062	−4·038
		1·030		1·579	0	2·970	1·579	0·010	−1·579	4·684	−2·980
		1·040		1·679	0	1·557	1·679	0·118	−1·679	3·263	−1·675
		1·050		1·775	0	0·567	1·775	0·234	−1·775	2·151	−0·800
		1·060		1·851	0	−0·036	1·851	0·337	−1·851	1·390	−0·301
		1·075		1·928	0	−0·482	1·928	0·460	−1·928	0·708	+0·022
		1·100		1·982	0	−0·642	1·982	0·593	−1·982	0·225	+0·049
		1·118		1·984	0	−0·582	1·984	0·650	−1·984	0·110	−0·068
14	—	1·118	→0	2·000	0	−0·667	2·000	0·667	−2·000	0	0
		1·155		1·964	0	−0·464	1·964	0·732	−1·964	−0·059	−0·268
		1·250		1·778	0	0·016	1·778	0·741	−1·778	0·099	−0·757
		1·414		1·500	0	0·333	1·500	0·667	−1·500	0·250	−1·000
		1·200	→0	1·879	0	−0·197	1·879	0·750	−1·879	0·012	−0·553
			0·20	1·809	0·048	−0·096	1·786	0·704	−1·834	0·088	−0·590
			0·30	1·734	0·094	0·019	1·685	0·654	−1·779	0·175	−0·639
			0·40	1·650	0·138	0·157	1·570	0·603	−1·708	0·276	−0·705
		1·400	→0	1·520	0	0·319	1·520	0·673	−1·520	0·243	−0·992
			0·20	1·505	0·020	0·330	1·496	0·662	−1·517	0·253	−0·986
			0·30	1·486	0·044	0·347	1·466	0·649	−1·511	0·265	−0·982
			0·40	1·461	0·072	0·370	1·428	0·632	−1·501	0·281	−0·978
			0·60	1·400	0·132	0·424	1·334	0·590	−1·466	0·324	−0·968

THIS DOCUMENT PROVIDED BY THE ABBOTT AEROSPACE
TECHNICAL LIBRARY
ABBOTTAEROSPACE.COM

TABLE 2c—*continued*

Method		M	$\bar{v}$	l_θ	l_z	$l_{\dot{\theta}}$	$l_{\dot{z}}$	$-m_\theta$	$m_z - l_\theta$	$-m_{\dot{\theta}}$	$m_{\dot{z}} - l_{\dot{\theta}}$
Ref.	$m(N)$			A	B	C	D	E	F	G	H
19	—	1·014	0·03	1·54	−0·002	2·80	1·53	0·025	−1·54	4·00	−2·82
		1·014	0·10	1·60	−0·011	2·49	1·59	0·119	−1·57	3·38	−2·61
		1·031		1·63	−0·014	2·86	1·61	0·175	−1·60	4·03	−3·03
		1·014	0·30	1·80	−0·012	1·40	1·71	0·468	−1·70	1·88	−1·83
		1·031		1·79	0·000	1·24	1·70	0·486	−1·70	1·75	−1·69
		1·050		1·85	0·005	1·16	1·77	0·595	−1·77	1·65	−1·71
		1·075		1·69	0·026	0·890	1·60	0·475	−1·62	1·42	−1·314
		1·118		1·70	0·092	0·088	1·60	0·521	−1·71	0·529	−0·540
		1·014	0·60	1·78	0·014	1·01	1·61	0·643	−1·62	1·08	−1·58
		1·050		1·79	0·046	0·888	1·61	0·689	−1·66	0·987	−1·491
		1·106		1·71	0·055	0·836	1·55	0·675	−1·60	0·884	−1·431

THIS DOCUMENT PROVIDED BY THE ABBOTT AEROSPACE
TECHNICAL LIBRARY
ABBOTTAEROSPACE.COM

TABLE 3a

Theoretical Derivatives for the Delta Wing ($A = 1{\cdot}5$) in Subsonic Flow.

Method		M	$\bar{\nu}$	l_θ	l_z	$l_{\dot\theta}$	$l_{\dot z}$	$-m_\theta$	$m_z - l_\theta$	$-m_{\dot\theta}$	$m_{\dot z} - l_{\dot\theta}$
Ref.	$m(N)$			A	B	C	D	E	F	G	H
4	11(3)	0·241	→0	0·921	0	2·087	0·921	1·089	−0·921	2·789	−3·176
		0·600		0·961	0	2·178	0·961	1·150	−0·961	2·967	−3·328
		0·800		1·012	0	2·292	1·012	1·228	−1·012	3·206	−3·520
		0·900		1·057	0	2·389	1·057	1·299	−1·057	3·426	−3·688
		0·950		1·092	0	2·456	1·092	1·356	−1·092	3·597	−3·812
		0·990		1·145	0	2·826	1·145	1·442	−1·145	4·299	−4·267
6	11(4)	0·990	0·015	1·124	0·000	2·421	1·124	1·418	−1·124	3·640	−3·839
	11(4)	0·970	0·050	1·088	−0·001	2·404	1·089	1·350	−1·086	3·514	−3·757
		0·990		1·124	−0·001	2·420	1·124	1·419	−1·122	3·612	−3·840
	11(4)	0·900	0·150	1·021	−0·009	2·305	1·028	1·237	−1·007	3·243	−3·556
		0·925		1·040	−0·008	2·337	1·045	1·267	−1·027	3·321	−3·616
		0·950		1·062	−0·008	2·372	1·066	1·306	−1·049	3·415	−3·688
		0·970		1·087	−0·007	2·401	1·088	1·350	−1·075	3·499	−3·758
		0·990		1·124	−0·006	2·412	1·121	1·424	−1·114	3·565	−3·835
	11(4)	0·900	0·300	0·999	−0·036	2·309	1·029	1·200	−0·944	3·256	−3·566
		0·950		1·049	−0·033	2·370	1·068	1·285	−0·997	3·414	−3·697
		0·990		1·120	−0·025	2·389	1·114	1·422	−1·079	3·514	−3·810
	10(6)	0·990		1·135	−0·029	2·475	1·129	1·416	−1·089	3·612	−3·890
7	7(3)	0·90	0·150	1·058	−0·010	2·461	1·066	1·255	−1·041	3·487	−3·734
	11(3)	0·90		1·050	−0·009	2·405	1·058	1·285	−1·035	3·453	−3·706
	7(3)	0·99	0·150	1·107	−0·010	2·557	1·108	1·304	−1·089	3·760	−3·870
	11(3)	0·99		1·123	−0·007	2·476	1·121	1·403	−1·109	3·677	−3·883
8	8(8)	0·80	0·015	1·007	0·000	2·281	1·007	1·204	−1·007	3·158	−3·485
		0·99		1·148	0·000	2·593	1·148	1·413	−1·148	3·919	−4·007
	12(6)	0·99	0·300	1·156	−0·025	2·457	1·138	1·480	−1·114	3·668	−3·922

THIS DOCUMENT PROVIDED BY THE ABBOTT AEROSPACE
TECHNICAL LIBRARY
ABBOTTAEROSPACE.COM

TABLE 3b

Theoretical Derivatives for the Delta Wing ($A = 1{\cdot}5$) in Sonic Flow.

Method		M	$\bar{\nu}$	l_θ	l_z	$l_{\dot\theta}$	$l_{\dot z}$	$-m_\theta$	$m_z - l_\theta$	$-m_{\dot\theta}$	$m_{\dot z} - l_{\dot\theta}$
Ref.	$m(N)$			A	B	C	D	E	F	G	H
9	—	1·0	→0	1·178	0	−∞	1·178	1·571	−1·178	−∞	∞
			0·01	1·178	0	1·920	1·178	1·571	−1·178	2·900	−3·490
			0·05	1·178	0	2·186	1·178	1·571	−1·178	3·300	−3·757
			0·15	1·178	0	2·368	1·178	1·571	−1·178	3·573	−3·939
10	Chap. 3	1·0	0·05	1·169	0·000	2·164	1·165	1·557	−1·169	3·265	−3·715
			0·15	1·164	−0·001	2·284	1·142	1·550	−1·160	3·439	−3·799
			0·30	1·175	−0·015	2·291	1·118	1·566	−1·144	3·441	−3·770
11	14(2)	1·0	0·05	1·294	0·000	2·376	1·291	1·687	−1·295	3·220	−4·058
	14(3)	1·0	0·05	1·278	0·001	2·058	1·274	1·766	−1·280	3·004	−3·816
			0·15	1·259	0·002	2·325	1·235	1·734	−1·264	3·505	−4·018
			0·30	1·258	−0·002	2·329	1·197	1·743	−1·260	3·495	−3·967

THIS DOCUMENT PROVIDED BY THE ABBOTT AEROSPACE
TECHNICAL LIBRARY
ABBOTTAEROSPACE.COM

TABLE 3c

Theoretical Derivatives for the Delta Wing ($A = 1{\cdot}5$) in Supersonic Flow.

Method		M	$\bar{\nu}$	l_θ	l_z	$l_{\dot\theta}$	$l_{\dot z}$	$-m_\theta$	$m_z - l_\theta$	$-m_{\dot\theta}$	$m_{\dot z} - l_{\dot\theta}$
Ref.	$m(N)$			A	B	C	D	E	F	G	H
15	—	1·009	→0	1·172	0	1·985	1·172	1·563	−1·172	2·977	−3·548
		1·010		1·172	0	2·001	1·172	1·562	−1·172	3·001	−3·563
		1·035		1·160	0	2·126	1·160	1·546	−1·160	3·188	−3·672
		1·077		1·142	0	2·139	1·142	1·523	−1·142	3·208	−3·662
		1·133		1·121	0	2·096	1·121	1·495	−1·121	3·144	−3·591
		1·281		1·074	0	1·936	1·074	1·433	−1·074	2·904	−3·369
		1·462		1·024	0	1·748	1·024	1·365	−1·024	2·621	−3·113
		1·667		0·973	0	1·565	0·973	1·297	−0·973	2·347	−2·862
		1·133	0·150	1·120	−0·001	2·100	1·111	1·494	−1·118	3·151	−3·578
		1·281		1·075	−0·001	1·934	1·070	1·434	−1·073	2·901	−3·359
		1·462		1·025	−0·001	1·746	1·021	1·367	−1·023	2·618	−3·107
		1·462	0·300	1·028	−0·005	1·741	1·014	1·371	−1·020	2·610	−3·091
18	7(3)	1·010	0·150	1·135	0·003	1·982	1·115	1·553	−1·139	3·003	−3·503
		1·075		1·083	0·002	1·875	1·069	1·474	−1·085	2·834	−3·328
	7(3)	1·010	0·300	1·128	−0·006	2·095	1·092	1·545	−1·117	3·190	−3·584
		1·075		1·082	−0·002	1·895	1·045	1·475	−1·079	2·866	−3·311
		1·150		1·034	−0·002	1·784	1·006	1·402	−1·028	2·684	−3·142
19	—	1·010	0·150	1·13	0·001	2·12	1·11	1·51	−1·13	3·28	−3·60
		1·030		1·14	0·001	2·12	1·12	1·52	−1·14	3·20	−3·61
		1·075		1·14	0·001	2·10	1·12	1·52	−1·14	3·18	−3·59
		1·150		1·11	0·000	2·02	1·10	1·47	−1·11	3·06	−3·47
		1·010	0·300	1·14	−0·004	2·12	1·09	1·55	−1·13	3·24	−3·59
		1·030		1·13	−0·006	2·12	1·08	1·50	−1·12	3·20	−3·56
		1·075		1·14	−0·005	2·10	1·10	1·52	−1·13	3·18	−3·56

THIS DOCUMENT PROVIDED BY THE ABBOTT AEROSPACE
TECHNICAL LIBRARY
ABBOTTAEROSPACE.COM

TABLE 4a

Theoretical Derivatives for the Symmetrical Tapered Wing ($A = 4{\cdot}33$) in Subsonic and Sonic Flow.

Method		M	$\bar{\nu}$	l_θ	l_z	$l_{\dot\theta}$	$l_{\dot z}$	$-m_\theta$	$m_z - l_\theta$	$-m_{\dot\theta}$	$m_{\dot z} - l_{\dot\theta}$
Ref.	$m(N)$			A	B	C	D	E	F	G	H
4	11(3)	0·60	→0	2·167	0	1·742	2·167	1·071	−2·167	1·502	−2·813
		0·80		2·474	0	1·464	2·474	1·206	−2·474	1·728	−2·670
		0·90		2·763	0	0·979	2·763	1·324	−2·763	2·101	−2·303
		0·95		2·997	0	0·421	2·997	1·406	−2·997	2·772	−1·827
		0·99		3·306	0	−0·075	3·306	1·451	−3·306	6·375	−1·376
6	11(4)	0·990	0·063	3·289	0·019	−1·174	3·253	1·603	−3·283	4·025	−0·419
	11(4)	0·900	0·190	2·677	0·056	1·197	2·581	1·320	−2·670	2·037	−2·498
		0·925		2·787	0·069	0·909	2·670	1·391	−2·779	2·176	−2·274
		0·950		2·915	0·090	0·387	2·766	1·508	−2·908	2·312	−1·852
		0·970		2·996	0·117	−0·389	2·815	1·666	−3·000	2·138	−1·200
		0·990		2·999	0·139	−1·055	2·810	1·758	−3·029	1·335	−0·592
	11(4)	0·900	0·380	2·651	0·166	1·226	2·362	1·415	−2·624	2·011	−2·560
		0·950		2·662	0·244	0·493	2·311	1·644	−2·699	1·598	−1·944
		0·990		2·603	0·272	0·246	2·254	1·647	−2·687	1·165	−1·672
7	7(3)	0·90	0·190	2·742	0·056	1·281	2·640	1·332	−2·730	2·255	−2·596
	11(3)			2·737	0·056	1·278	2·636	1·341	−2·725	2·251	−2·603
	7(3)	0·99	0·190	2·967	0·178	−2·460	2·734	1·823	−3·022	0·564	0·786
	11(3)			3·000	0·172	−2·217	2·771	1·826	−3·043	0·932	0·534

THIS DOCUMENT PROVIDED BY THE ABBOTT AEROSPACE
TECHNICAL LIBRARY
ABBOTTAEROSPACE.COM

TABLE 4a—*continued*

Method		M	$\bar{v}$	l_θ	l_z	$l_{\dot{\theta}}$	$l_{\dot{z}}$	$-m_\theta$	$m_z - l_\theta$	$-m_{\dot{\theta}}$	$m_{\dot{z}} - l_{\dot{\theta}}$
Ref.	$m(N)$			A	B	C	D	E	F	G	H
8	8(2)	0·900	0·380	2·722	0·166	1·324	2·424	1·429	−2·689	2·091	−2·681
	12(6)	0·990		2·661	0·280	0·182	2·291	1·741	−2·738	1·311	−1·664
	12(6)	0·600	0·633	1·925	−0·061	2·114	1·867	0·889	−1·771	1·674	−3·086
		0·800		2·436	0·097	1·905	2·128	1·200	−2·281	1·981	−3·102
		0·850		2·614	0·204	1·586	2·171	1·416	−2·494	2·009	−2·904
		0·900		2·584	0·317	1·073	2·072	1·656	−2·573	1·711	−2·466
		0·925		2·488	0·316	1·024	2·015	1·638	−2·515	1·529	−2·378
		0·950		2·493	0·327	0·994	2·013	1·657	−2·533	1·498	−2·351
		0·970		2·487	0·349	0·914	2·000	1·696	−2·554	1·407	−2·278
		0·990		2·476	0·354	0·894	1·994	1·696	−2·558	1·351	−2·244
11	14(3)	1·0	0·190	2·994	0·176	−2·246	2·773	1·859	−3·029	1·246	0·529
	14(2)	1·0	0·380	2·712	0·308	−0·045	2·294	1·744	−2·786	1·345	−1·443
	14(3)			2·514	0·321	−0·249	2·133	1·743	−2·633	0·900	−1·217
	14(4)			2·531	0·300	−0·086	2·158	1·695	−2·645	0·917	−1·338

THIS DOCUMENT PROVIDED BY THE ABBOTT AEROSPACE
TECHNICAL LIBRARY
ABBOTTAEROSPACE.COM

TABLE 4b

Theoretical Derivatives for the Symmetrical Tapered Wing ($A = 4{\cdot}33$) in Supersonic Flow.

Method		M	$\bar{\nu}$	l_θ	l_z	$l_{\dot\theta}$	$l_{\dot z}$	$-m_\theta$	$m_z - l_\theta$	$-m_{\dot\theta}$	$m_{\dot z} - l_{\dot\theta}$
Ref.	$m(N)$			A	B	C	D	E	F	G	H
16	—	1·035	→0	4·108	0	−14·572	4·108	2·436	−4·108	−9·705	12·136
		1·064		3·877	0	−8·760	3·877	2·647	−3·877	−7·323	6·113
		1·102		3·517	0	−4·796	3·517	2·575	−3·517	−4·396	2·222
		1·155		3·027	0	−1·974	3·027	2·282	−3·027	−1·885	−0·307
		1·414		1·893	0	+0·556	1·893	1·468	−1·893	+0·490	−2·024
17	—	1·155	0·095	2·975	0·039	−1·898	2·950	2·249	−3·012	−1·796	−0·326
		1·414		1·881	0·008	+0·557	1·876	1·474	−1·889	+0·496	−2·025
		1·105	0·190	2·941	0·202	−3·053	2·796	2·052	−3·117	−2·565	+1·133
		1·155		2·798	0·139	−1·550	2·706	2·065	−2·925	−1·404	−0·420
		1·250		2·367	0·073	−0·114	2·321	1·809	−2·435	−0·124	−1·647
		1·414		1·867	0·033	+0·569	1·847	1·459	−1·899	+0·510	−2·006
		1·105	0·380	2·262	0·366	−0·628	1·922	1·465	−2·503	−0·044	−0·523
		1·155		2·333	0·354	−0·529	2·062	1·609	−2·619	−0·289	−0·813
		1·414		1·818	0·118	+0·614	1·741	1·405	−1·927	+0·562	−1·940
18	10(4)	1·102	0·019	3·536	0·003	−4·787	3·534	2·563	−3·539	−4·258	2·226
			0·190	2·883	0·194	−2·855	2·738	1·913	−3·041	−2·150	1·086
			0·380	2·129	0·261	+0·038	1·828	1·299	−2·242	+0·756	−1·071
	8(4)	1·414	0·019	1·897	0·000	0·534	1·897	1·462	−1·898	+0·473	−1·995
			0·190	1·862	0·033	0·566	1·841	1·423	−1·893	+0·510	−1·967

THIS DOCUMENT PROVIDED BY THE ABBOTT AEROSPACE
TECHNICAL LIBRARY
ABBOTTAEROSPACE.COM

TABLE 4b—*continued*

Method		M	$\bar{v}$	l_θ	l_z	$l_{\dot{\theta}}$	$l_{\dot{z}}$	$-m_\theta$	$m_z - l_\theta$	$-m_{\dot{\theta}}$	$m_{\dot{z}} - l_{\dot{\theta}}$
Ref.	$m(N)$			A	B	C	D	E	F	G	H
19	—	1·010	0·019	3·65	0·005	−11·71	3·66	1·62	−3·65	3·87	10·07
		1·035		4·02	0·006	−14·24	4·02	2·36	−4·02	−8·88	11·88
		1·010	0·063	3·49	0·035	−5·06	3·43	1·90	−3·49	3·86	3·20
		1·035		3·60	0·057	−10·52	3·55	2·02	−3·63	−5·28	8·54
		1·010	0·190	2·96	0·174	−2·16	2·73	1·88	−3·01	0·804	0·44
		1·035		2·91	0·168	−2·02	2·69	1·87	−2·96	0·844	0·32
		1·064		2·79	0·208	−3·18	2·60	1·64	−2·91	−1·033	1·72
		1·080		2·85	0·221	−3·42	2·67	1·82	−3·02	−2·40	1·78
		1·102		2·89	0·201	−3·05	2·74	1·87	−3·05	−2·13	1·32
		1·035	0·380	2·59	0·315	−0·175	2·16	1·79	−2·72	0·886	−1·295

THIS DOCUMENT PROVIDED BY THE ABBOTT AEROSPACE
TECHNICAL LIBRARY
ABBOTTAEROSPACE.COM

TABLE 5

Experimental Derivatives for the Rectangular Wing ($A = 2$).

(a) Sealed 36 in. × 14 in. tunnel. Axis $x_0 = 0{\cdot}42\bar{c}$

M	$\bar{v}$	l_θ	$l_{\dot\theta}$	$-m_\theta$	$-m_{\dot\theta}$	
0·603	0·120	1·436	0·536	−0·309	0·261	Uncorrected
0·708	0·104	1·499	0·461	−0·335	0·329	
0·812	0·092	1·590	0·459	−0·378	0·482	
0·868	0·086	1·695	0·366	−0·362	0·783	
0·603	0·120	1·352	0·649	−0·296	0·237	Corrected
0·708	0·104	1·405	0·610	−0·320	0·295	
0·812	0·092	1·478	0·663	−0·360	0·427	
0·868	0·086	1·564	0·653	−0·345	0·702	

(b) Slotted 36 in. × 14 in. tunnel. Axis $x_0 = 0{\cdot}42\bar{c}$

M	$\bar{v}$	l_θ	$l_{\dot\theta}$	$-m_\theta$	$-m_{\dot\theta}$	
0·595	0·120	1·429	0·552	−0·302	0·234	Uncorrected
0·695	0·104	1·465	0·494	−0·328	0·319	
0·794	0·092	1·577	0·542	−0·364	0·405	
0·844	0·087	1·654	0·521	−0·390	0·548	
0·891	0·084	1·702	0·551	−0·324	0·739	
0·939	0·078	0·599	1·940	−0·530	1·159	
0·986	0·076	1·119	0·322	−0·462	0·904	
1·092	0·071	1·741	−1·127	−0·119	0·274	

(c) Slotted 25 in. × 20 in. tunnel. Axis $x_0 = 0{\cdot}42\bar{c}$

M	$\bar{v}$	l_θ	$l_{\dot\theta}$	$-m_\theta$	$-m_{\dot\theta}$	
1·000	0·158	1·013	0·808	−0·445	0·775	Uncorrected
1·100	0·148	1·643	−0·456	−0·139	0·377	
1·180	0·140	1·654	−0·683	−0·076	0·286	

THIS DOCUMENT PROVIDED BY THE ABBOTT AEROSPACE
TECHNICAL LIBRARY
ABBOTTAEROSPACE.COM

TABLE 5—*continued*

Experimental Derivatives for the Rectangular Wing ($A = 2$).

(d) Effect of axis position ($M \approx 0{\cdot}85$)

M	$\bar{\nu}$	Axis $x_0/\bar{c}$	Tunnel	Uncorrected		Corrected	
				$-m_\theta$	$-m_{\dot\theta}$	$-m_\theta$	$-m_{\dot\theta}$
0·868	0·084	0·17	Sealed	0·062	0·809	0·046	0·795
	0·086	0·42	36 in. ×	−0·362	0·783	−0·345	0·702
	0·081	0·67	14 in.	−0·788	0·892	−0·739	0·727
0·844	0·084	0·17	Slotted	0·005	0·647		
	0·087	0·42	36 in. ×	−0·390	0·548		
	0·082	0·67	14 in.	−0·778	0·639		

TABLE 6

Experimental Derivatives for the Symmetrical Tapered Wing ($A = 4{\cdot}33$).

(a) Sealed 36 in. × 14 in. tunnel. Axis $x_0 = 0{\cdot}79\bar{c}$

M	$\bar{\nu}$	l_θ	$l_{\dot\theta}$	$-m_\theta$	$-m_{\dot\theta}$	
0·603	0·078	2·243	−0·737	−0·622	0·751	Uncorrected
0·708	0·068	2·427	−1·230	−0·659	0·999	
0·812	0·060	2·659	−2·170	−0·709	1·464	
0·868	0·057	2·936	−3·687	−0·667	1·786	
0·603	0·078	2·083	−0·200	−0·583	0·604	Corrected
0·708	0·068	2·238	−0·497	−0·615	0·798	
0·812	0·060	2·426	−1·059	−0·657	1·161	
0·868	0·057	2·650	−2·012	−0·617	1·401	

(b) Slotted 36 in. × 14 in. tunnel. Axis $x_0 = 0{\cdot}79\bar{c}$

M	$\bar{\nu}$	l_θ	$l_{\dot\theta}$	$-m_\theta$	$-m_{\dot\theta}$	
0·595	0·078	2·255	−0·796	−0·604	0·759	Uncorrected
0·695	0·068	2·408	−1·256	−0·648	1·006	
0·794	0·060	2·610	−1·814	−0·696	1·312	
0·844	0·056	2·732	−2·374	−0·695	1·563	
0·891	0·054	2·973	−3·893	−0·613	1·611	
0·939	0·051	2·447	−2·686	−0·645	1·580	
0·986	0·049	2·580	−2·743	−0·581	1·904	
1·037	0·047	2·586	−3·839	−0·571	2·353	
1·092	0·046	2·536	−3·625	−0·571	2·985	

THIS DOCUMENT PROVIDED BY THE ABBOTT AEROSPACE
TECHNICAL LIBRARY
ABBOTTAEROSPACE.COM

TABLE 6—*continued*

Experimental Derivatives for the Symmetrical Tapered Wing ($A = 4{\cdot}33$).

(c) Sealed 25 in. × 20 in. tunnel. Axis $x_0 = 0{\cdot}79\bar{c}$

M	$\bar{v}$	l_θ	$l_{\dot{\theta}}$	$-m_\theta$	$-m_{\dot{\theta}}$	
0·600	0·078	2·178	−0·318	−0·629	0·616	Uncorrected
0·700	0·067	2·328	−0·482	−0·665	0·801	
0·800	0·059	2·515	−1·041	−0·697	1·151	
0·850	0·056	2·740	−1·885	−0·653	1·406	
0·600	0·078	2·021	−0·140	−0·592	0·568	Corrected
0·700	0·067	2·145	−0·251	−0·624	0·734	
0·800	0·059	2·292	−0·677	−0·652	1·046	
0·850	0·056	2·473	−1·330	−0·610	1·270	

(d) Perforated 25 in. × 20 in. tunnel. Axis $x_0 = 0{\cdot}79\bar{c}$

M	$\bar{v}$	l_θ	$l_{\dot{\theta}}$	$-m_\theta$	$-m_{\dot{\theta}}$	
0·600	0·078	2·013	0·176	−0·574	0·402	Uncorrected
0·700	0·068	2·078	0·100	−0·597	0·551	
0·800	0·060	2·307	−0·520	−0·626	0·856	
0·850	0·056	2·463	−0·657	−0·616	1·074	
0·900	0·054	2·423	−1·053	−0·543	1·215	
1·000	0·049	2·245	−1·310	−0·581	1·987	
1·100	0·045	2·495	−3·975	−0·590	2·885	
1·200	0·042	2·740	−6·385	−0·438	1·277	
1·300	0·040	2·378	−3·603	−0·083	0·144	
1·400	0·038	2·056	−2·369	−0·045	0·078	

(e) Effect of axis position ($M = 0{\cdot}9$)

M	$\bar{v}$	$x_0/\bar{c}$	Tunnel	$-m_\theta$	$-m_{\dot{\theta}}$	
0·891	0·056	0·395	Slotted	0·509	0·359	Uncorrected
	0·055	0·480	36 in.	0·261	0·594	
	0·054	0·790	× 14 in.	−0·613	1·611	
	0·052	1·185		−1·706	3·626	
0·900	0·056	0·395	Perforated	0·448	0·730	Uncorrected
	0·054	0·790	25 in.	−0·543	1·215	
	0·052	1·185	× 20 in.	−1·557	2·416	

THIS DOCUMENT PROVIDED BY THE ABBOTT AEROSPACE
TECHNICAL LIBRARY
ABBOTTAEROSPACE.COM

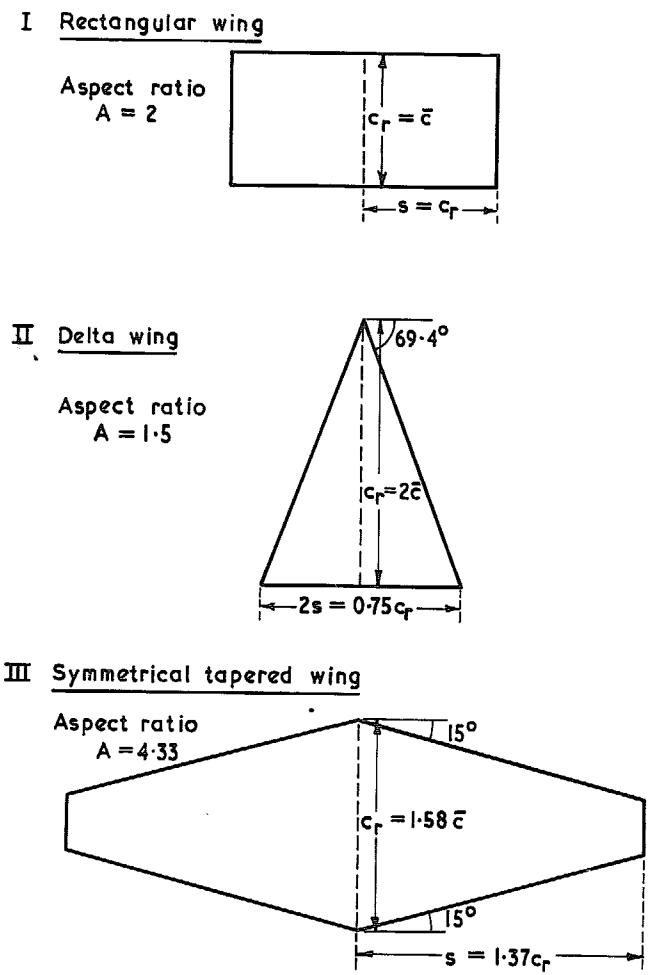

FIG. 1. Planforms for transonic theory and experiment.

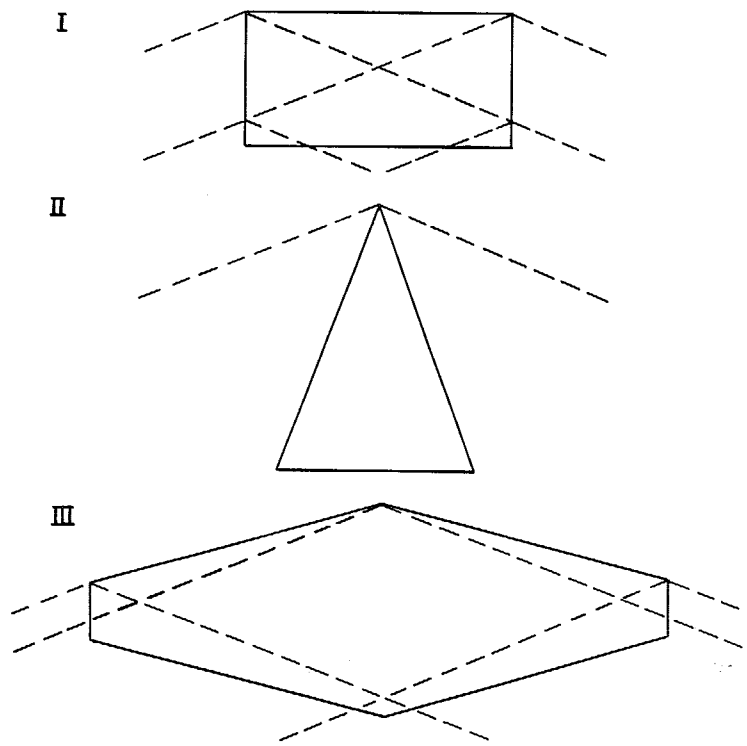

Conditions	I	II	III
Sonic leading edge	M = 1·000	M = 2·848	M = 1·035
Tip Mach lines intersect on wing	M < 1·414		M < 1·102
Wing tips interact	M < 1·118		

FIG. 2. Critical Mach numbers in supersonic theory for three planforms and Mach lines at $M = 1{\cdot}075$.

THIS DOCUMENT PROVIDED BY THE ABBOTT AEROSPACE
TECHNICAL LIBRARY
ABBOTTAEROSPACE.COM

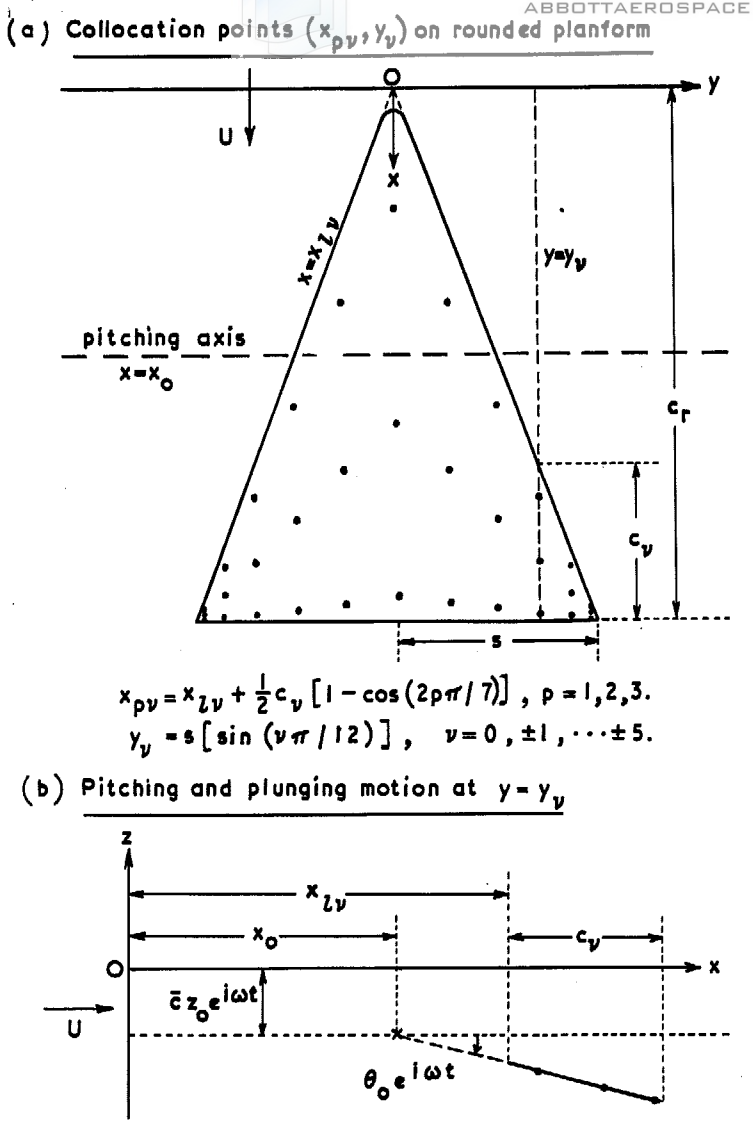

FIG. 3. Representation of the oscillating delta wing in subsonic flow ($m = 11$, $N = 3$).

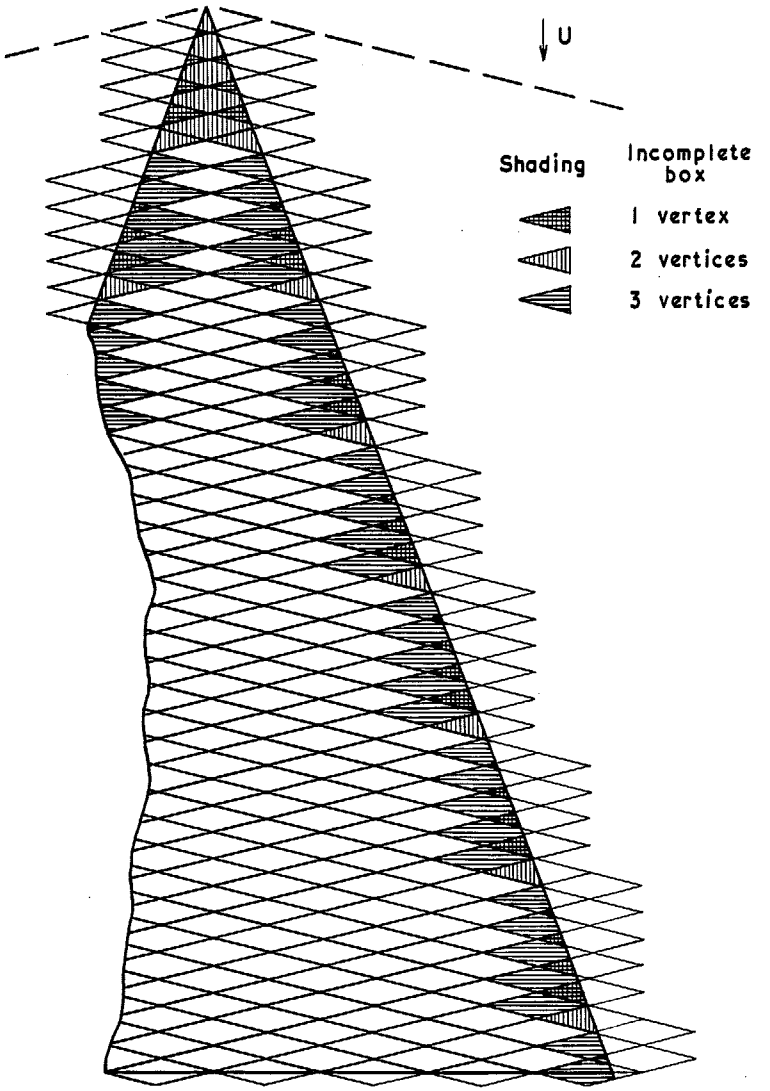

FIG. 4. Diamond grid for the delta wing in supersonic flow (Ref. 19, $M = 1{\cdot}03$).

THIS DOCUMENT PROVIDED BY THE ABBOTT AEROSPACE
TECHNICAL LIBRARY
ABBOTTAEROSPACE.COM

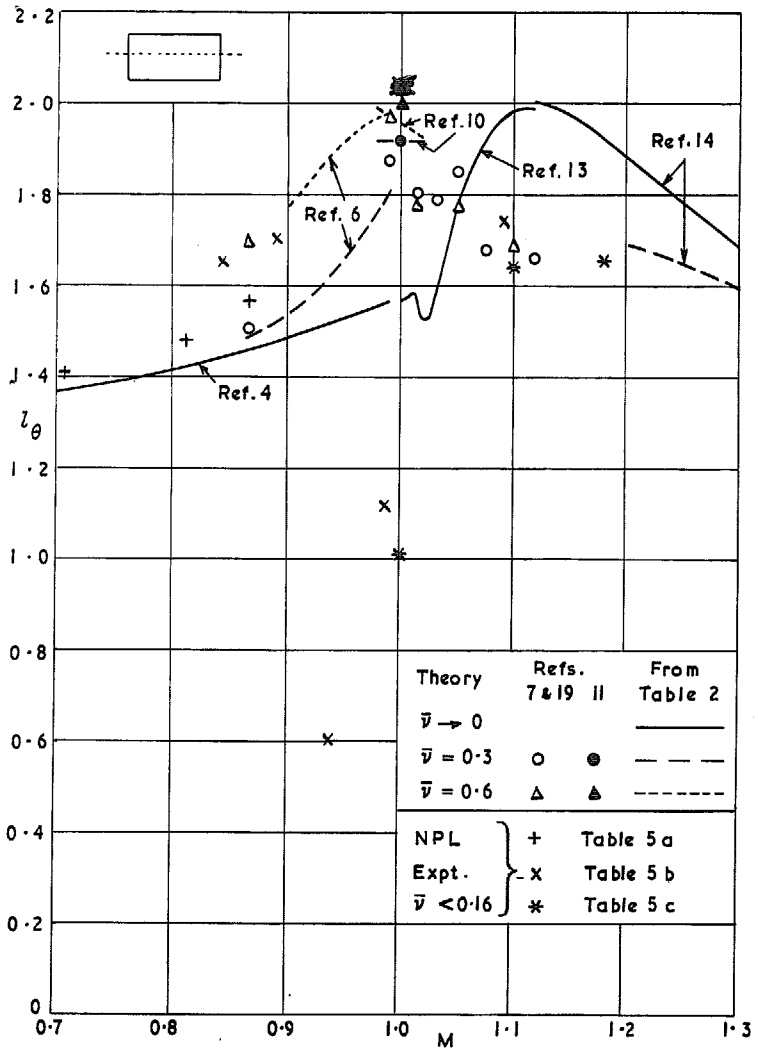

FIG. 5. l_θ against M for rectangular wing ($x_0 = 0{\cdot}42\bar{c}$).

Amended 28/4/69.

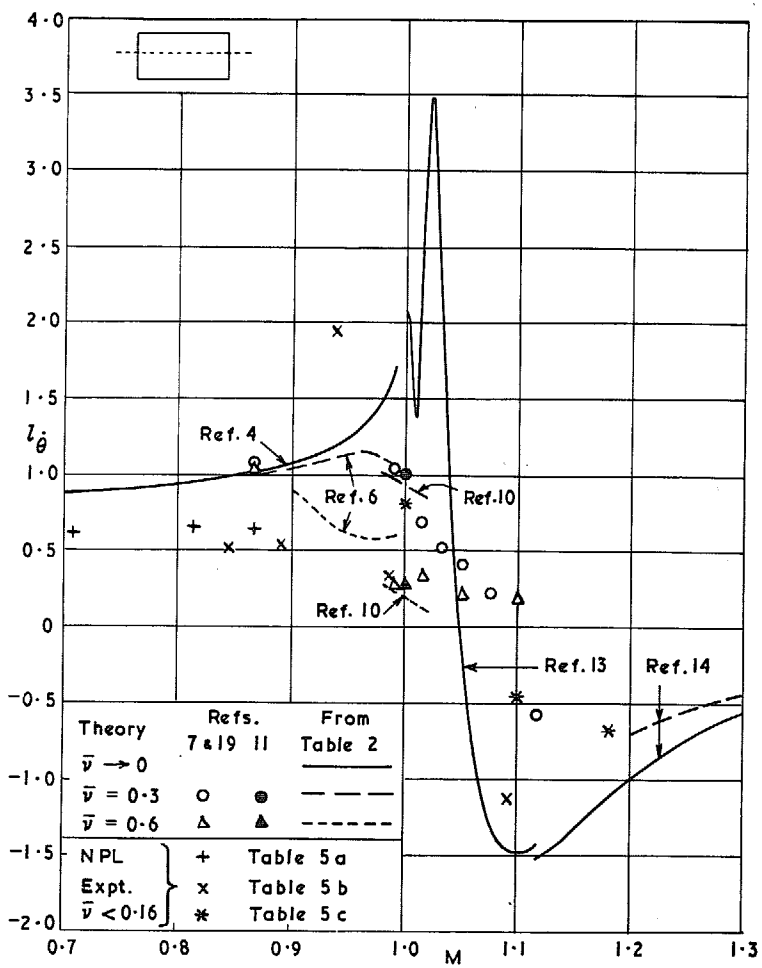

FIG. 6. $l_{\dot\theta}$ against M for rectangular wing ($x_0 = 0{\cdot}42\bar{c}$).

THIS DOCUMENT PROVIDED BY THE ABBOTT AEROSPACE
TECHNICAL LIBRARY
ABBOTTAEROSPACE.COM

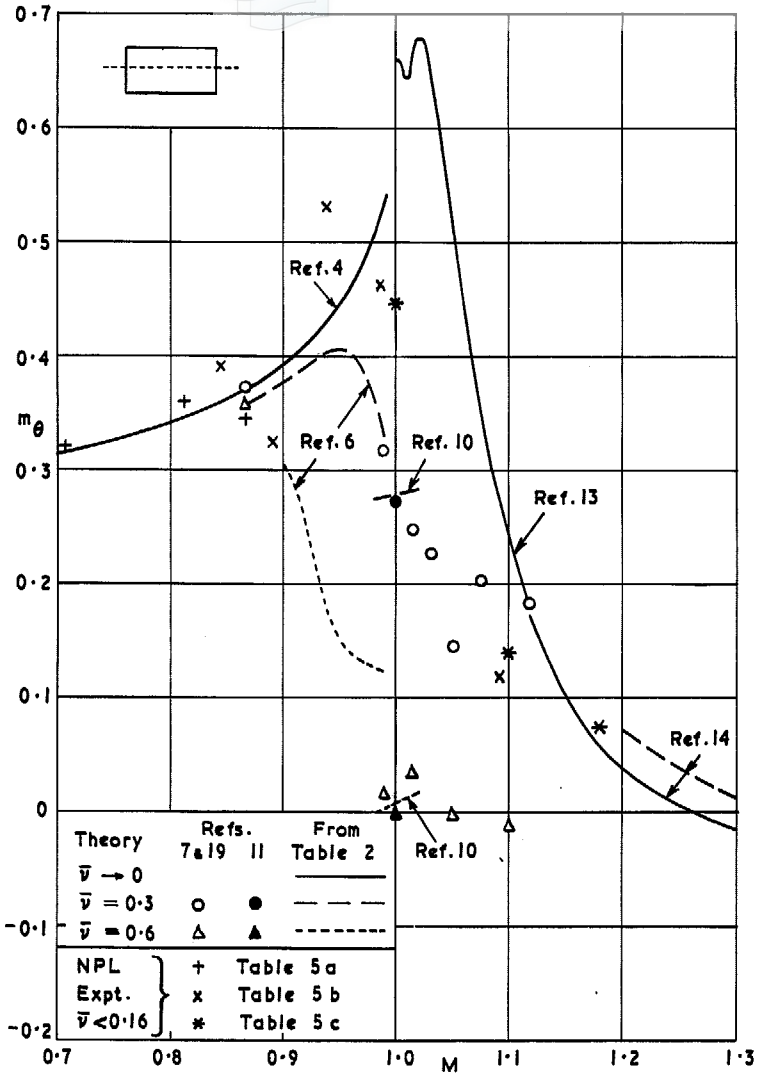

FIG. 7. m_θ against M for rectangular wing ($x_0 = 0{\cdot}42\bar{c}$).

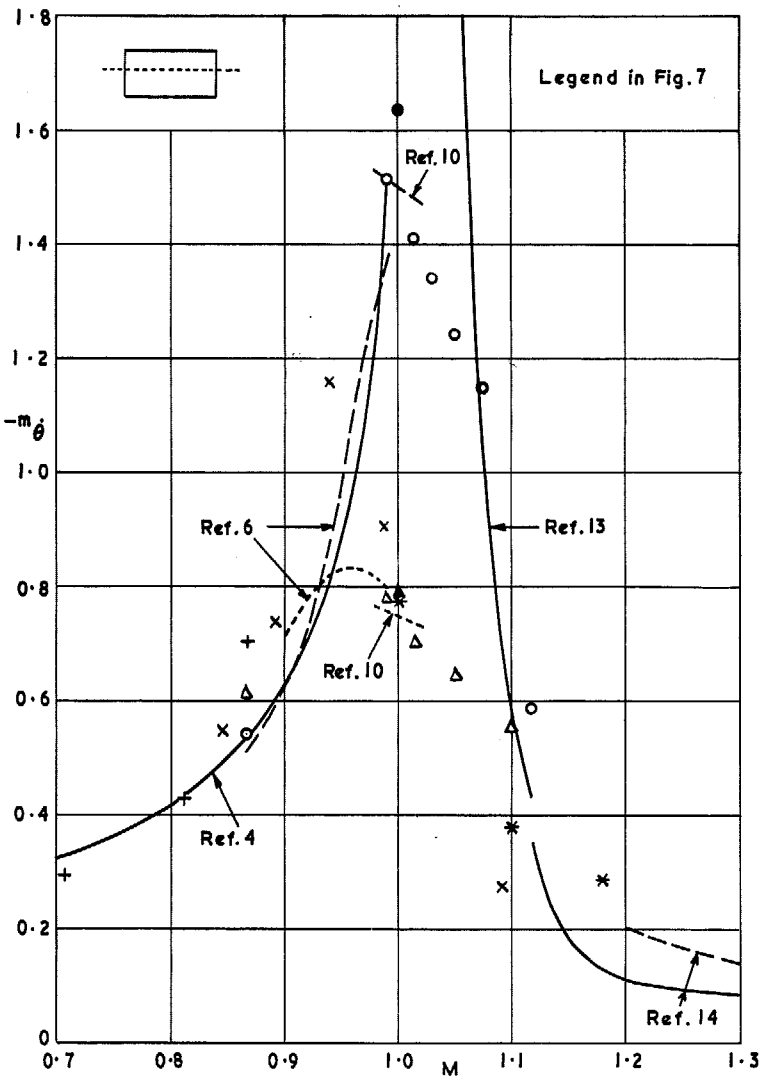

FIG. 8. $-m_{\dot\theta}$ against M for rectangular wing ($x_0 = 0{\cdot}42\bar{c}$).

THIS DOCUMENT PROVIDED BY THE ABBOTT AEROSPACE
TECHNICAL LIBRARY
ABBOTTAEROSPACE.COM

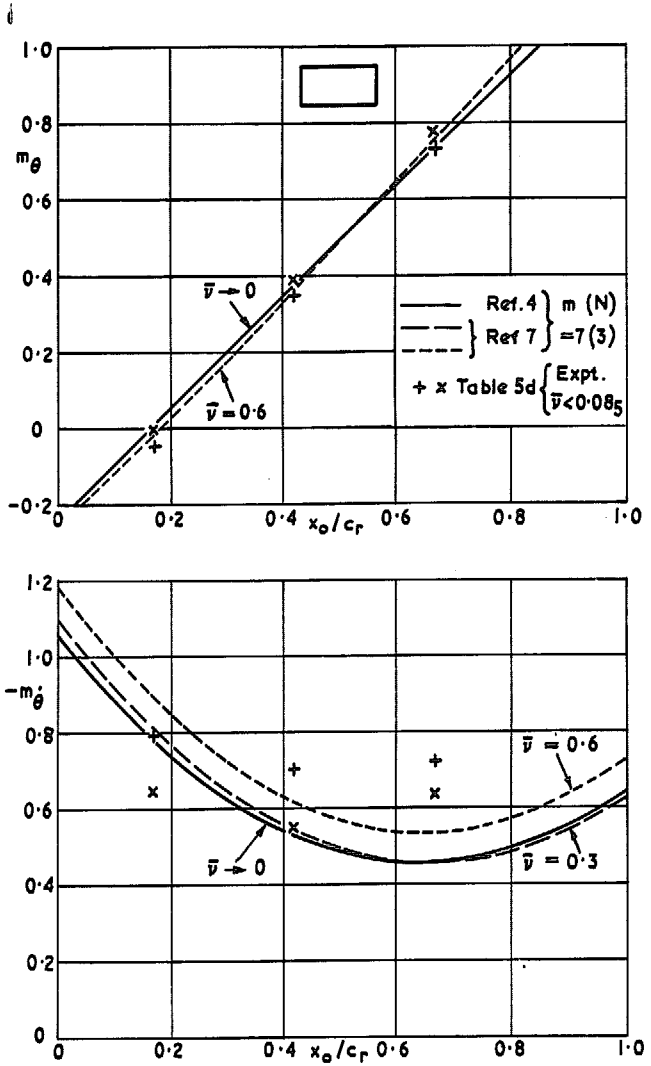

FIG. 9. m_θ and $-m_{\dot\theta}$ against x_0/c_r for rectangular wing at $M = 0{\cdot}866$.

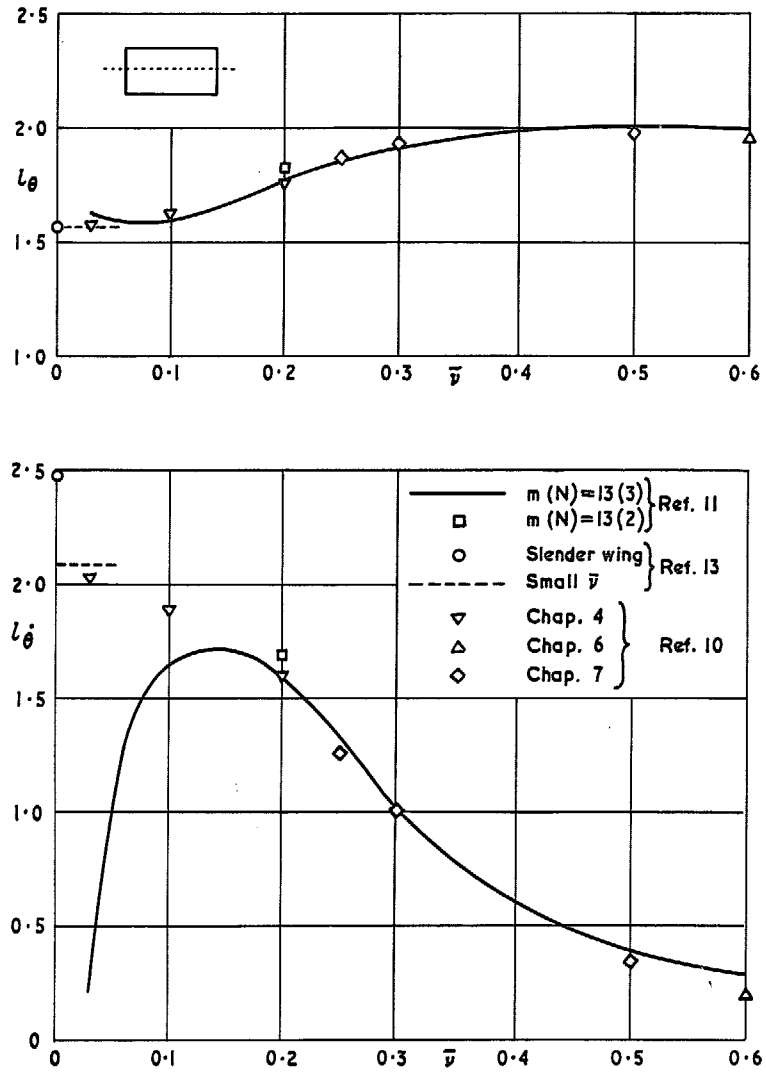

FIG. 10. l_θ and $l_{\dot\theta}$ against $\bar{\nu}$ for rectangular wing at $M = 1$ ($x_0 = 0{\cdot}42\bar{c}$).

THIS DOCUMENT PROVIDED BY THE ABBOTT AEROSPACE
TECHNICAL LIBRARY
ABBOTTAEROSPACE.COM

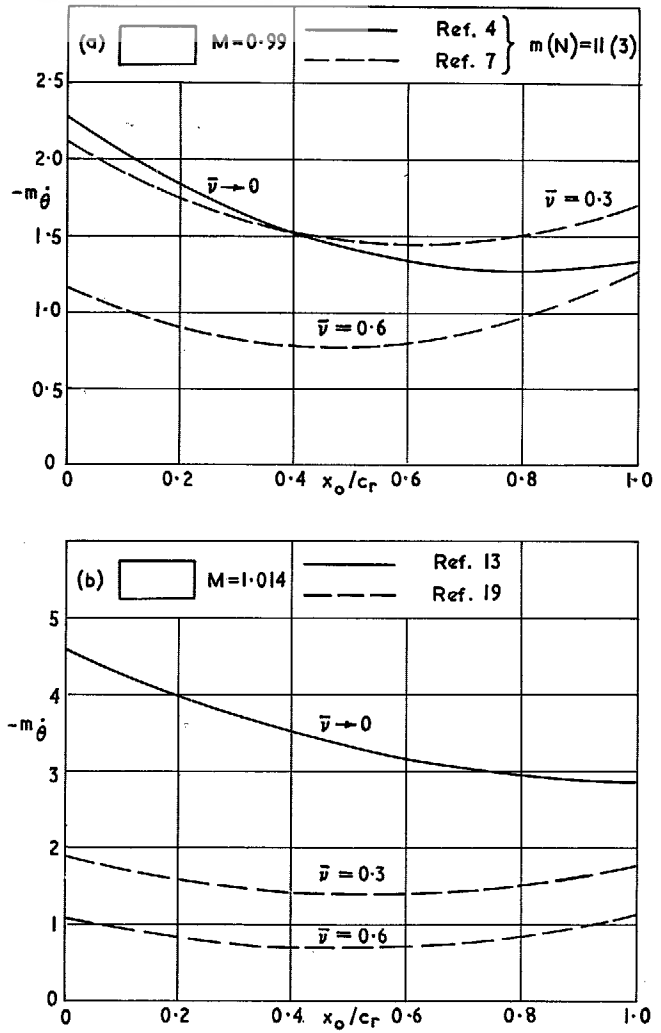

FIG. 11. $-m_{\dot{\theta}}$ against x_0/c_r for rectangular wing at $M = 0{\cdot}99$ and $M = 1{\cdot}014$.

THIS DOCUMENT PROVIDED BY THE ABBOTT AEROSPACE
TECHNICAL LIBRARY
ABBOTTAEROSPACE.COM

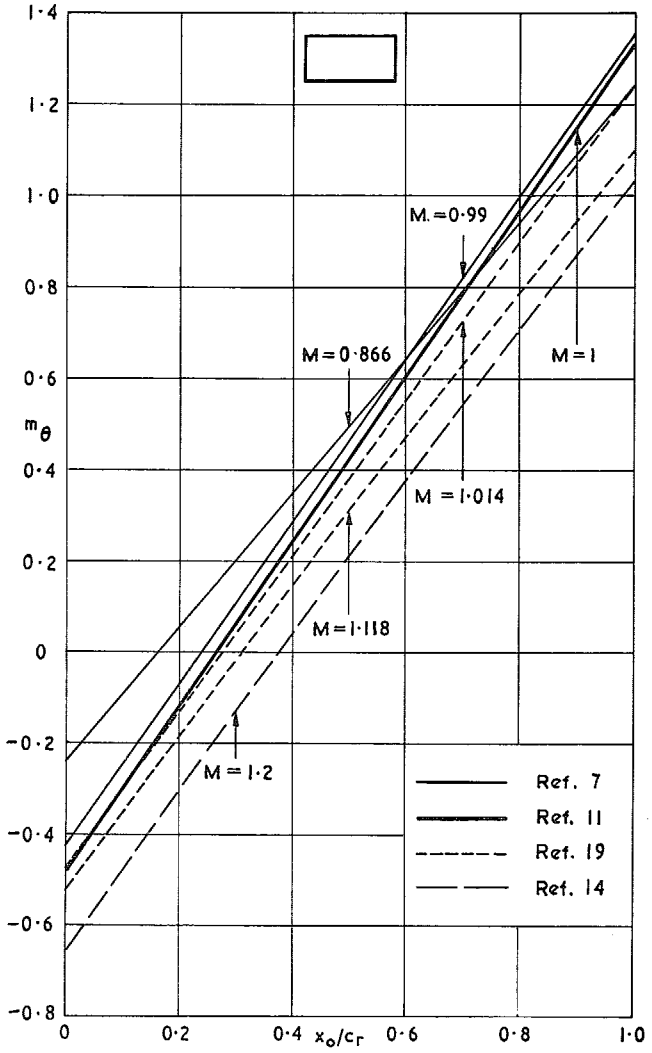

FIG. 12. m_θ against x_0/c_r for rectangular wing ($\bar{v} = 0{\cdot}3$).

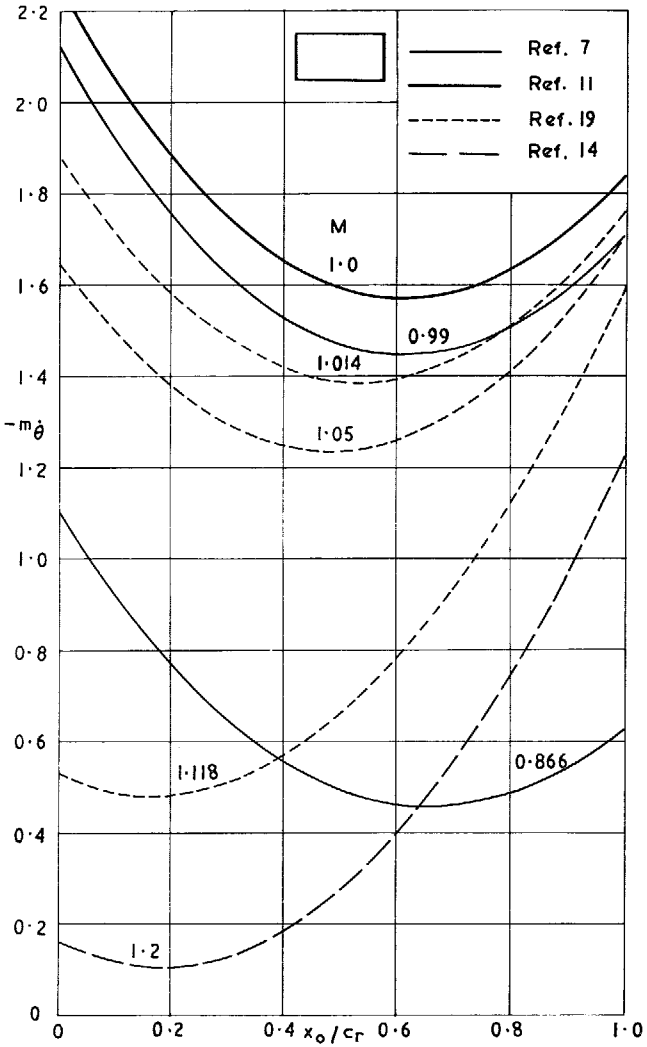

FIG. 13. $-m_{\dot\theta}$ against x_0/c_r for rectangular wing ($\bar{v} = 0{\cdot}3$).

THIS DOCUMENT PROVIDED BY THE ABBOTT AEROSPACE
TECHNICAL LIBRARY
ABBOTTAEROSPACE.COM

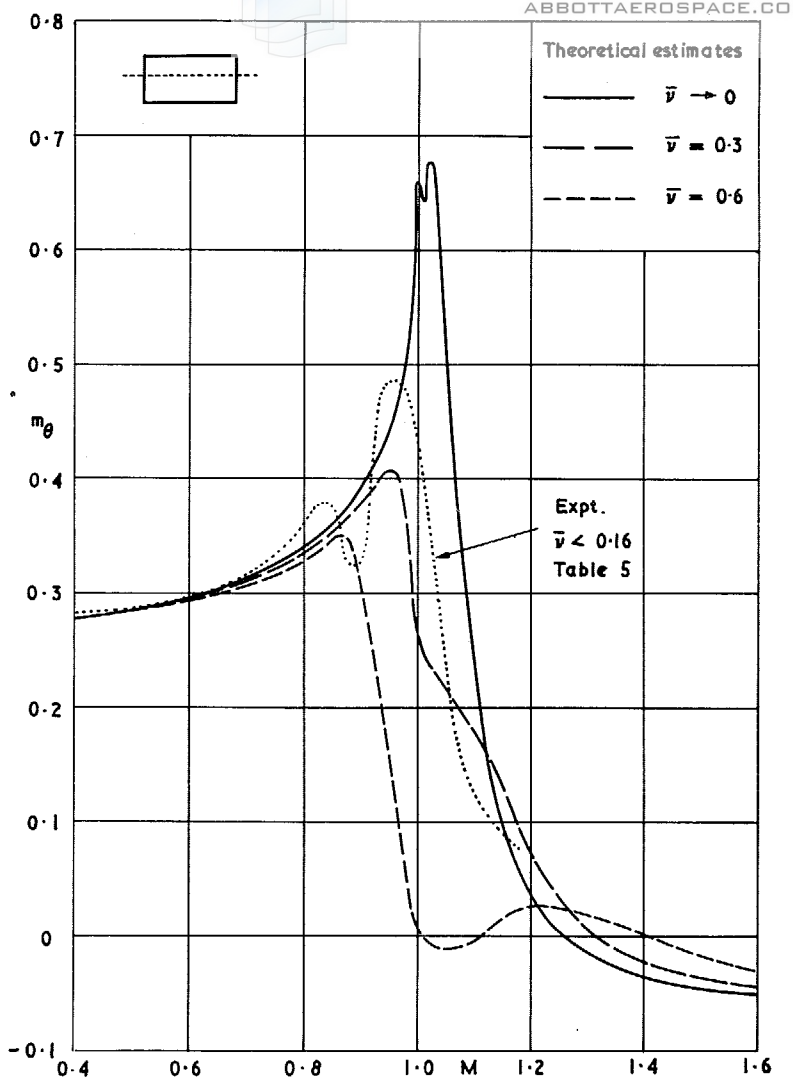

FIG. 14. Digest of theoretical and experimental m_θ for rectangular wing ($x_0 = 0{\cdot}42\bar{c}$).

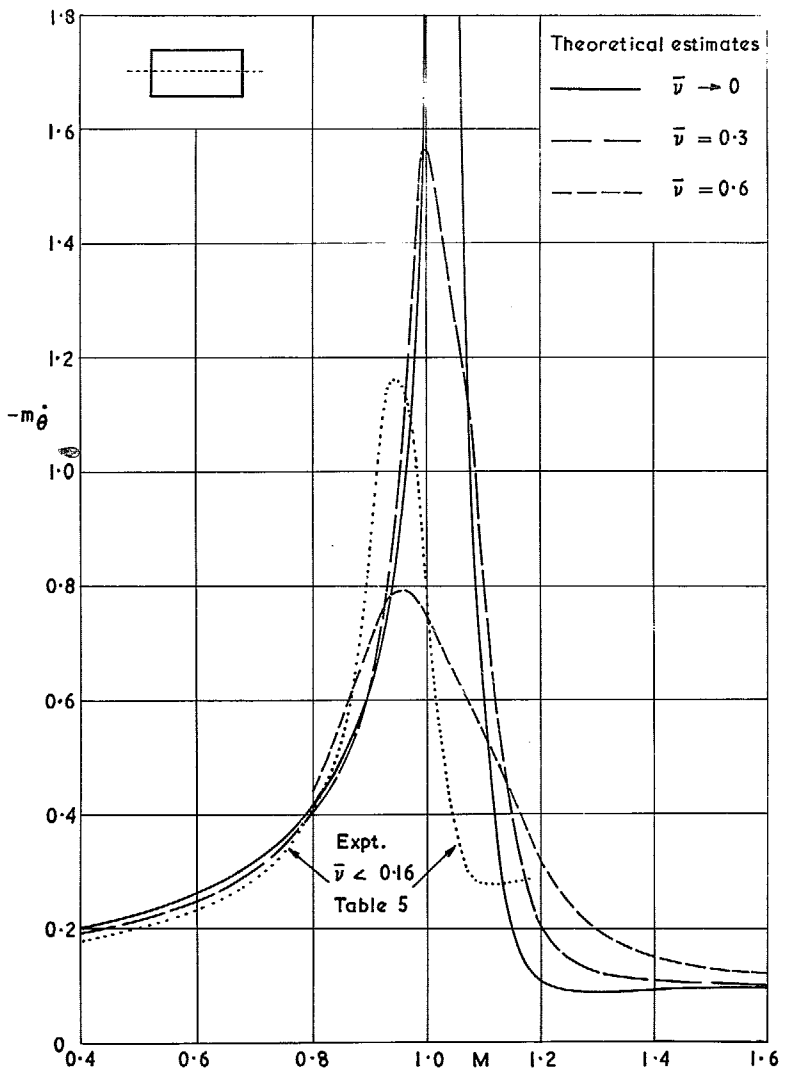

FIG. 15. Digest of theoretical and experimental $-m_{\dot\theta}$ for rectangular wing ($x_0 = 0{\cdot}42\bar{c}$).

THIS DOCUMENT PROVIDED BY THE ABBOTT AEROSPACE
TECHNICAL LIBRARY
ABBOTTAEROSPACE.COM

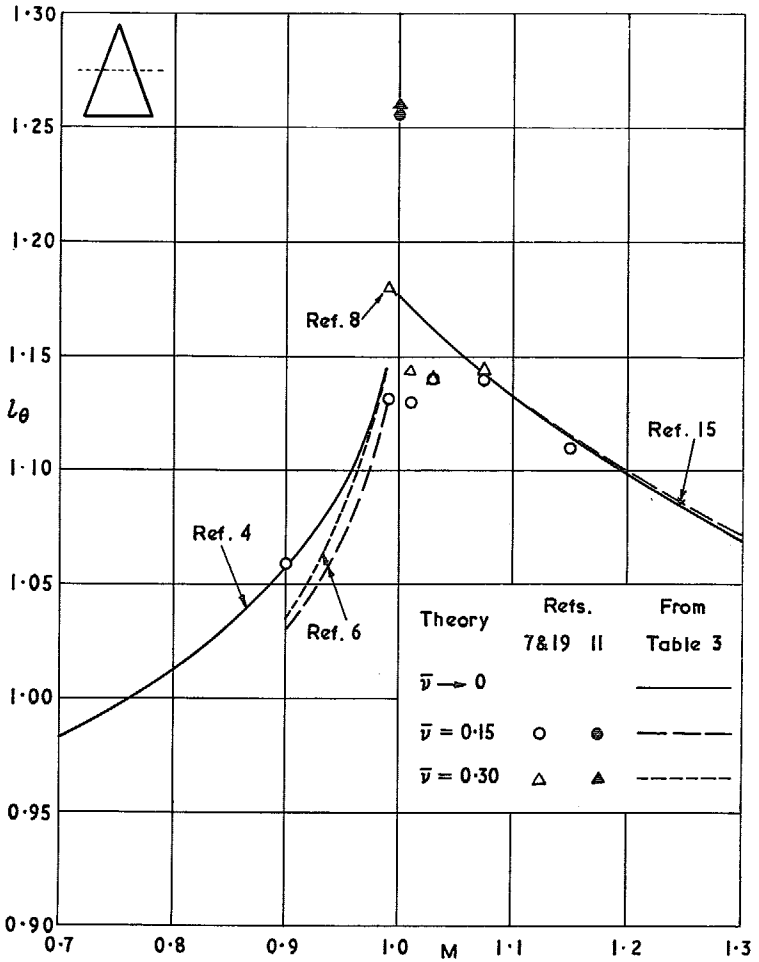

FIG. 16. l_θ against M for delta wing ($x_0 = \bar{c}$).

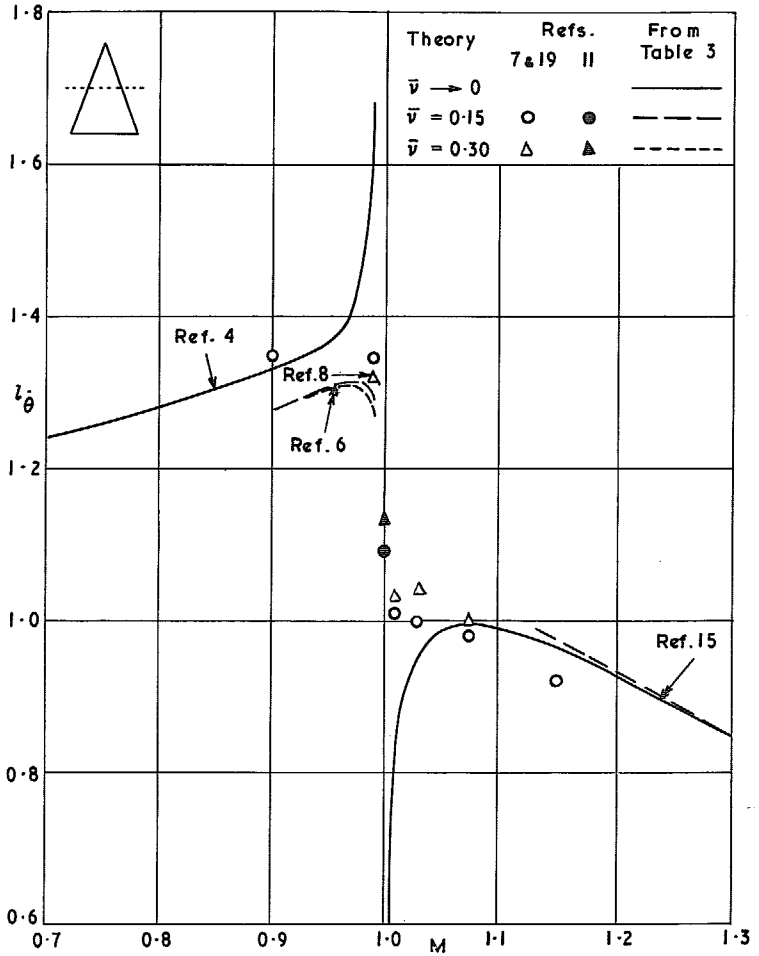

FIG. 17. $l_{\dot\theta}$ against M for delta wing ($x_0 = \bar{c}$).

THIS DOCUMENT PROVIDED BY THE ABBOTT AEROSPACE
TECHNICAL LIBRARY
ABBOTTAEROSPACE.COM

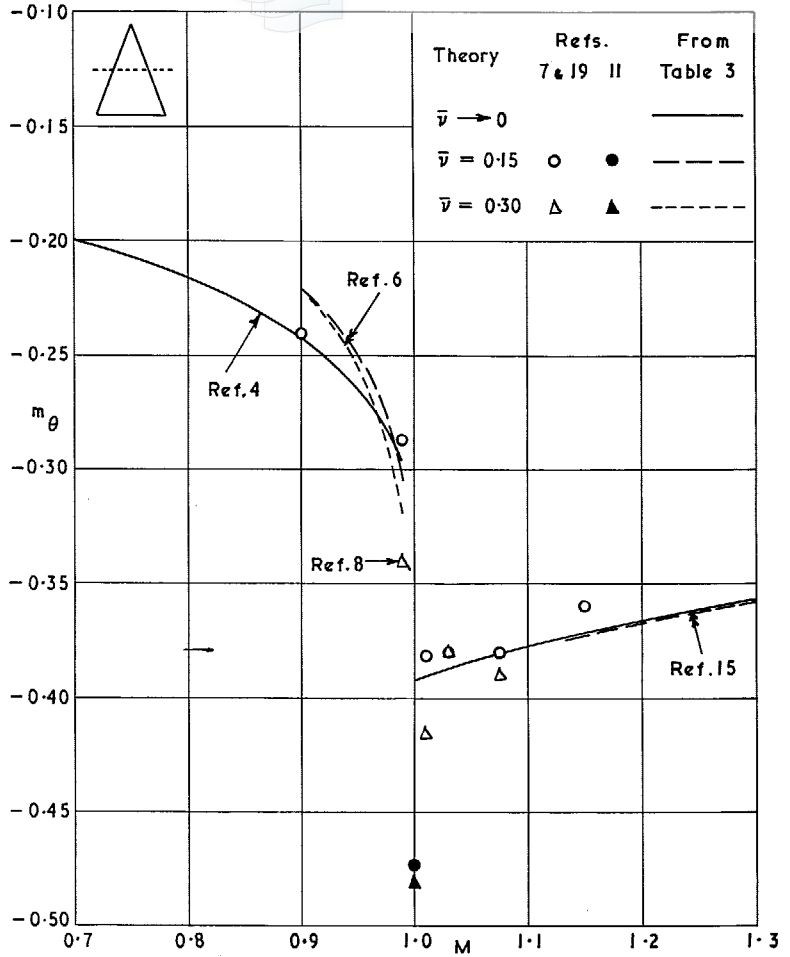

FIG. 18. m_θ against M for delta wing ($x_0 = \bar{c}$).

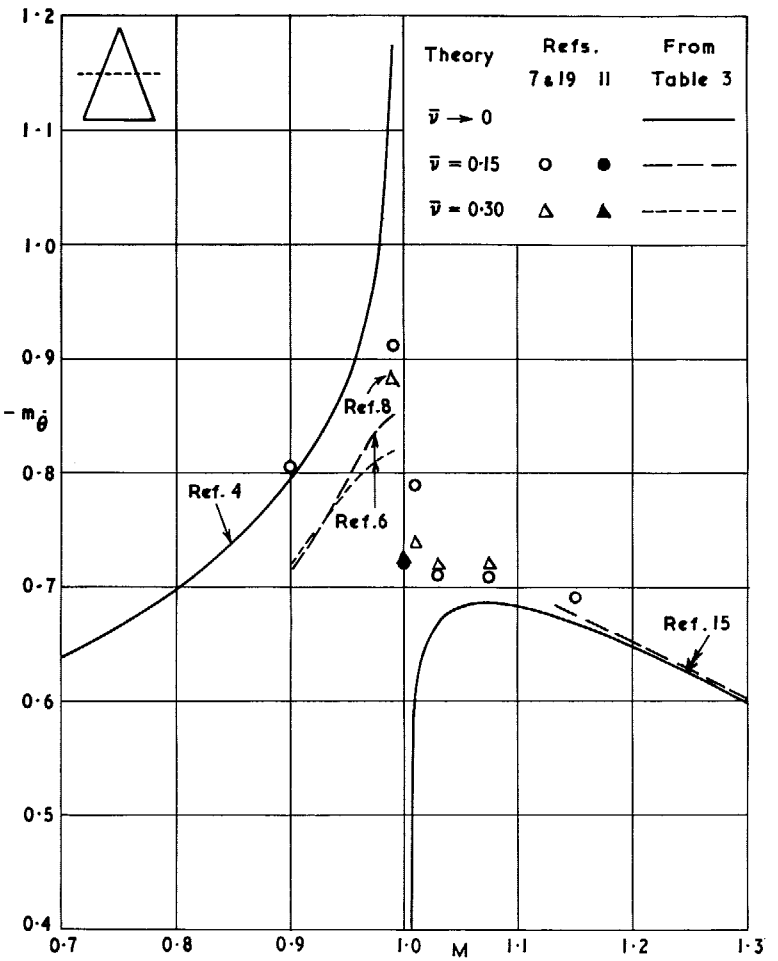

FIG. 19. $-m_{\dot\theta}$ against M for delta wing ($x_0 = \bar{c}$).

THIS DOCUMENT PROVIDED BY THE ABBOTT AEROSPACE
TECHNICAL LIBRARY
ABBOTTAEROSPACE.COM

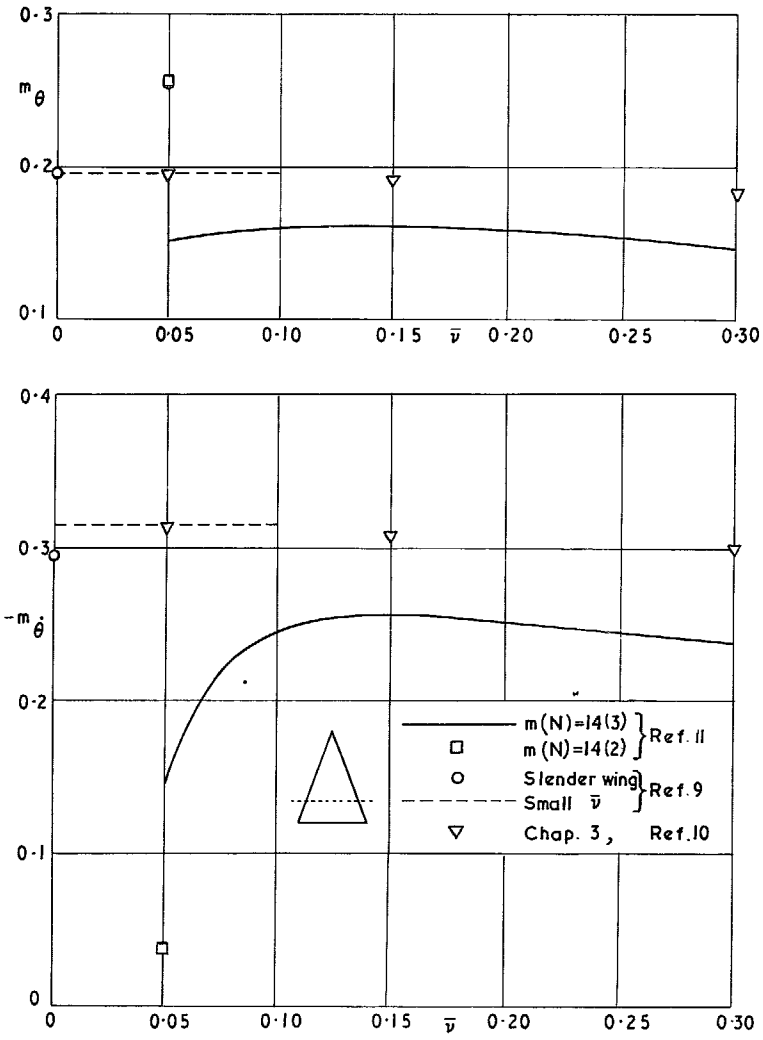

FIG. 20. m_θ and $-m_{\dot\theta}$ against $\bar\nu$ for delta wing at $M = 1$ ($x_0 = 1{\cdot}5\bar c$).

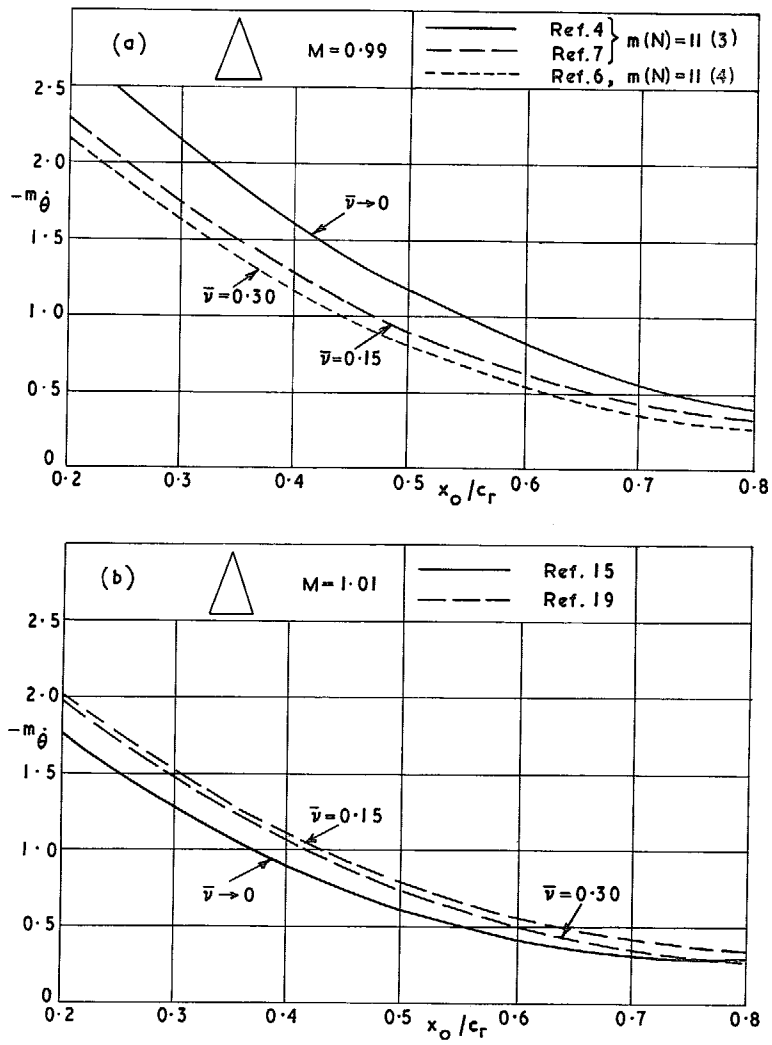

FIG. 21. $-m_{\dot\theta}$ against $x_0\ c_r$ for delta wing at $M = 0{\cdot}99$ and $M = 1{\cdot}01$.

THIS DOCUMENT PROVIDED BY THE ABBOTT AEROSPACE
TECHNICAL LIBRARY
ABBOTTAEROSPACE.COM

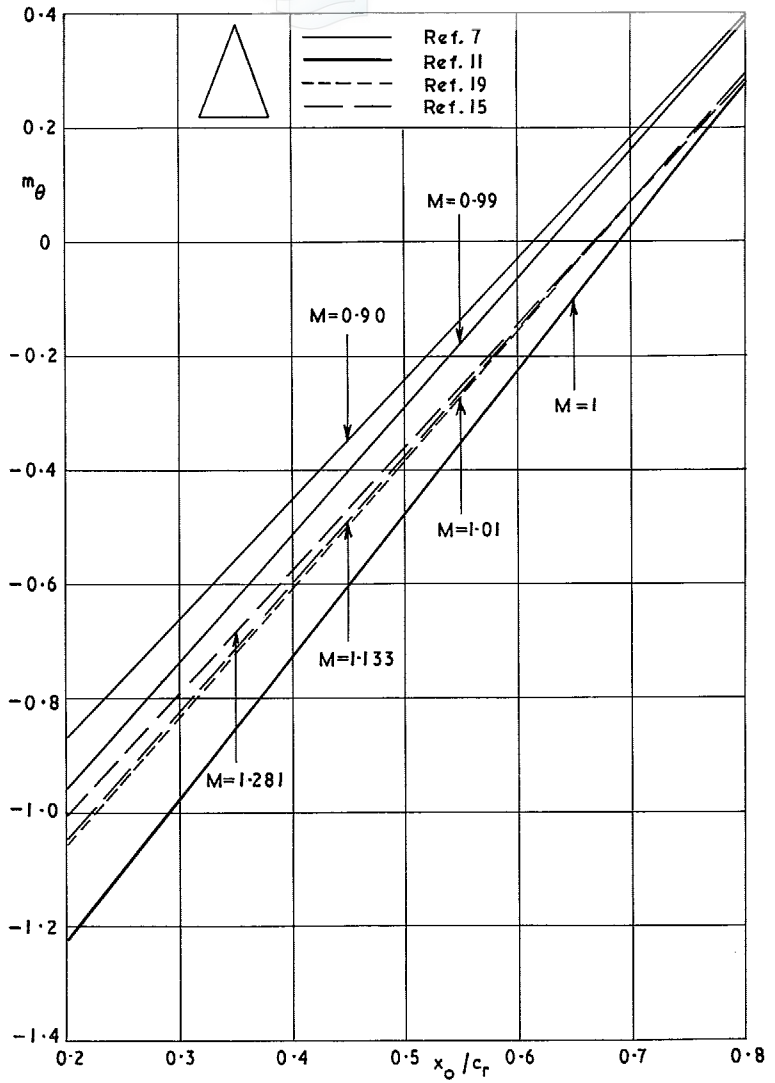

FIG. 22. m_θ against x_0/c_r for delta wing ($\bar{v} = 0{\cdot}15$).

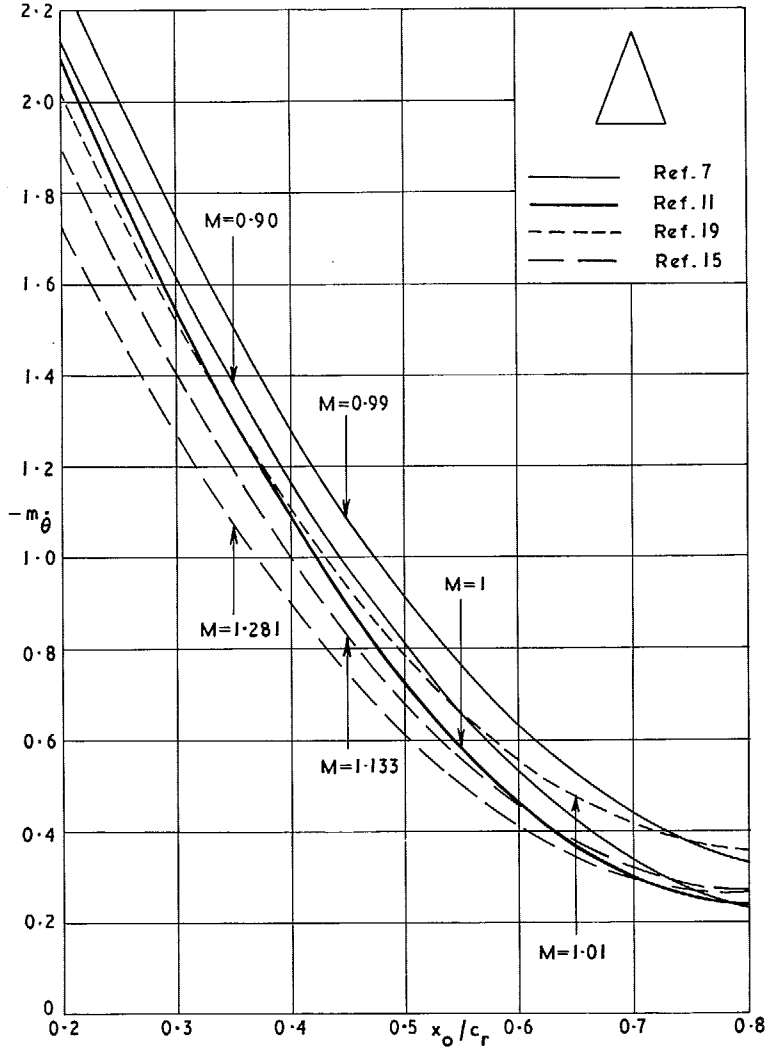

FIG. 23. $-m_{\dot\theta}$ against x_0/c_r for delta wing ($\bar{v} = 0{\cdot}15$).

THIS DOCUMENT PROVIDED BY THE ABBOTT AEROSPACE
TECHNICAL LIBRARY
ABBOTTAEROSPACE.COM

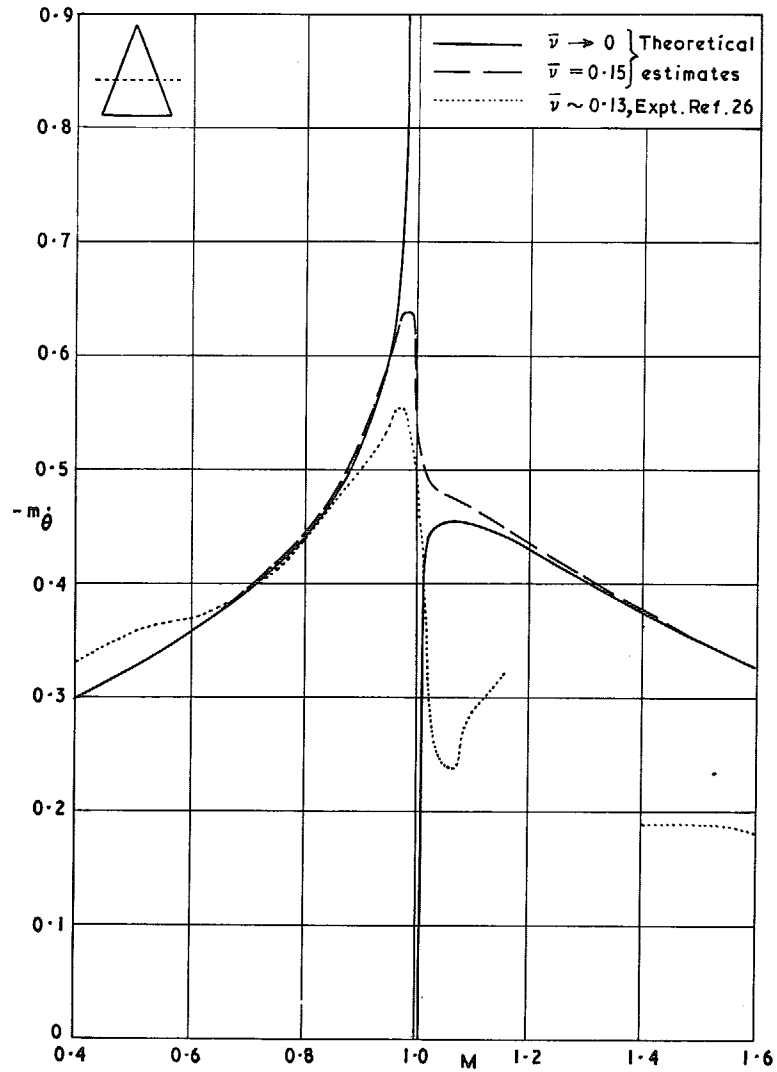

FIG. 24. Digest of theoretical and experimental $-m_{\dot{\theta}}$ for delta wing ($x_0 = 1{\cdot}2\bar{c}$).

THIS DOCUMENT PROVIDED BY THE ABBOTT AEROSPACE
TECHNICAL LIBRARY
ABBOTTAEROSPACE.COM

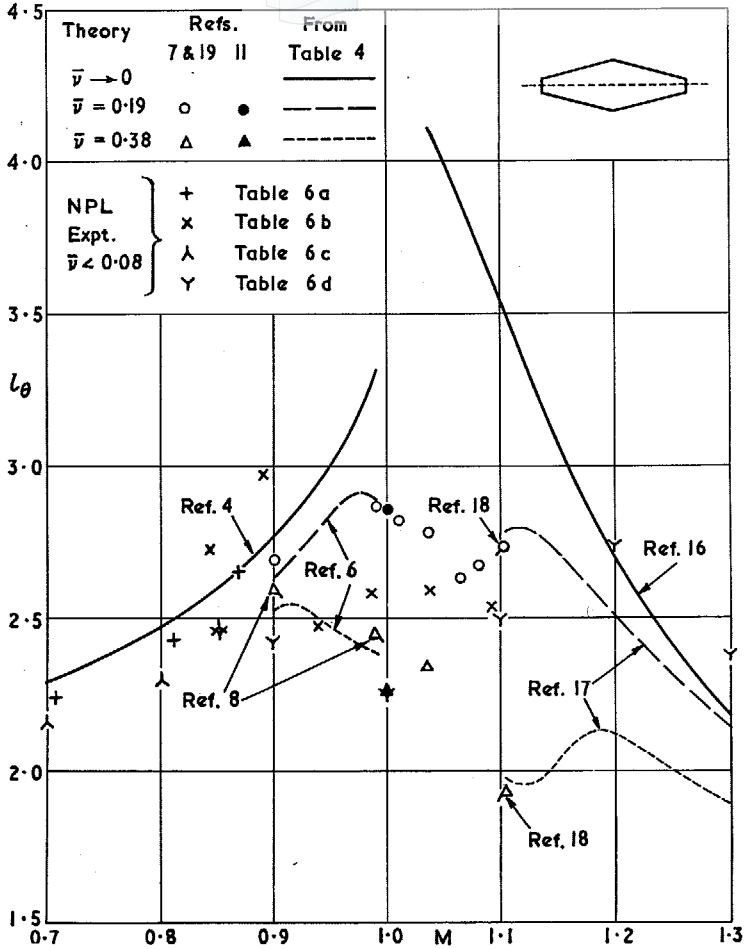

FIG. 25. l_θ against M for symmetrical tapered wing ($x_0 = 0{\cdot}79\bar{c}$).

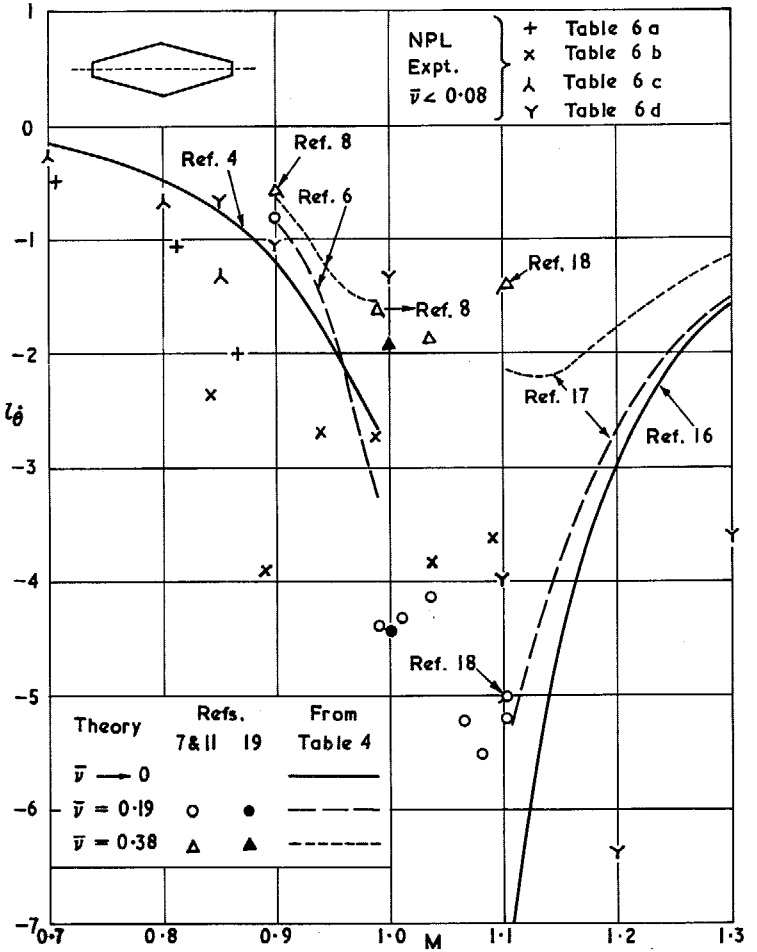

FIG. 26. $l_{\dot{\theta}}$ against M for symmetrical tapered wing ($x_0 = 0{\cdot}79\bar{c}$).

THIS DOCUMENT PROVIDED BY THE ABBOTT AEROSPACE
TECHNICAL LIBRARY
ABBOTTAEROSPACE.COM

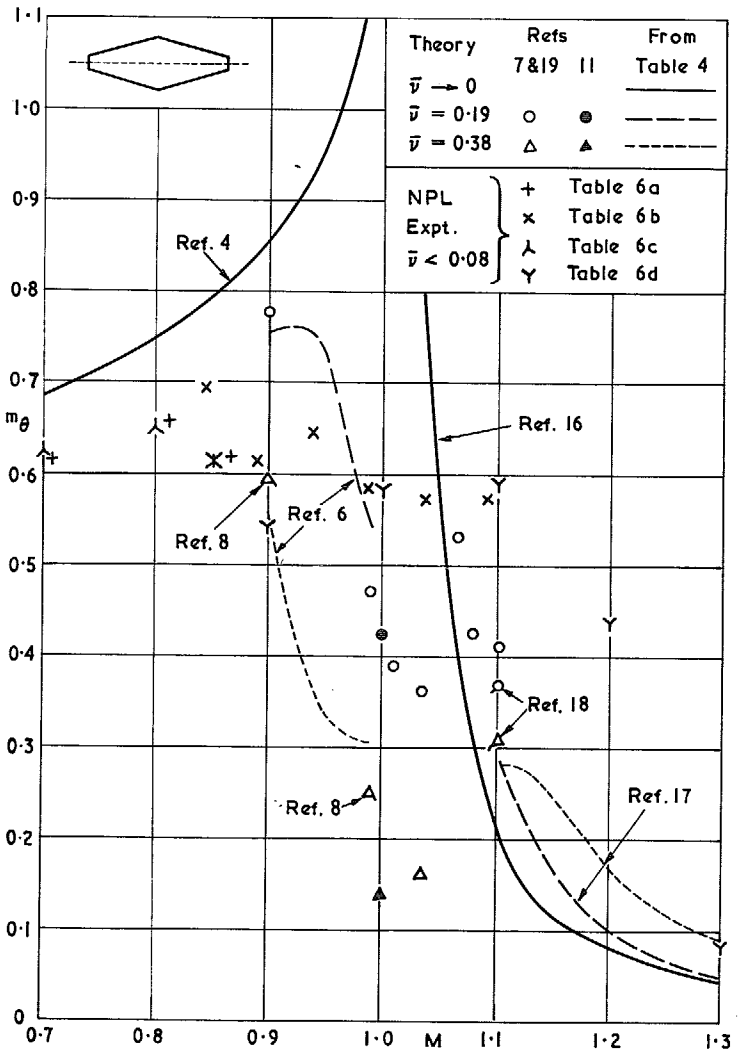

FIG. 27. m_θ against M for symmetrical tapered wing ($x_0 = 0{\cdot}79\bar{c}$).

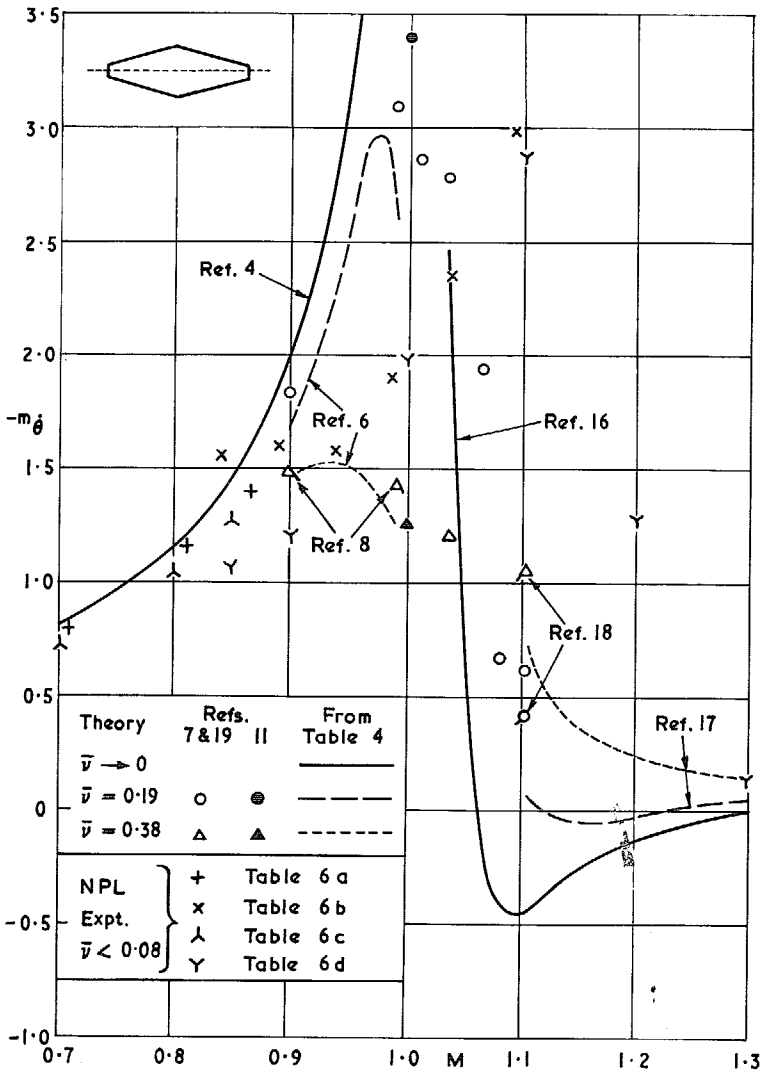

FIG. 28. $-m_{\dot\theta}$ against M for symmetrical tapered wing ($x_0 = 0{\cdot}79\bar{c}$).

THIS DOCUMENT PROVIDED BY THE ABBOTT AEROSPACE
TECHNICAL LIBRARY
ABBOTTAEROSPACE.COM

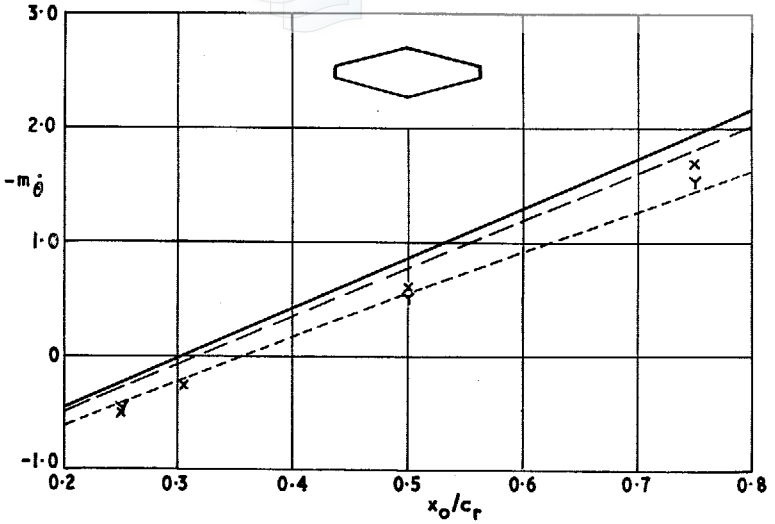

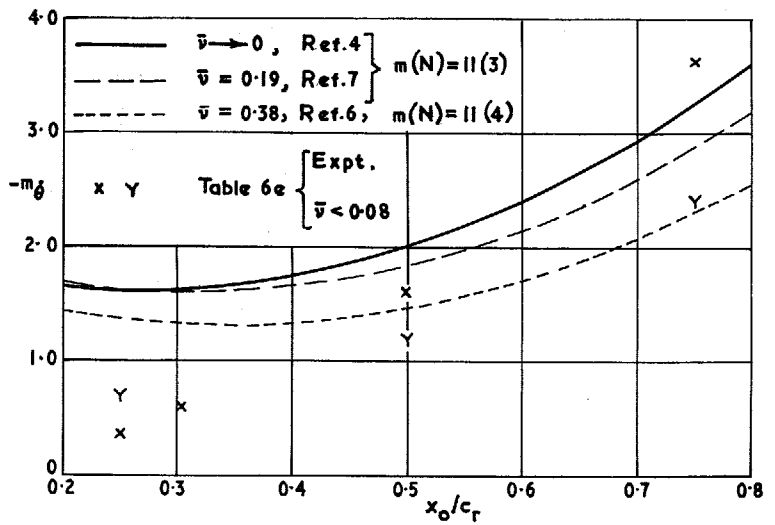

FIG. 29. m_θ and $-m_{\dot\theta}$ against x_0/c_r for symmetrical tapered wing at $M = 0{\cdot}9$.

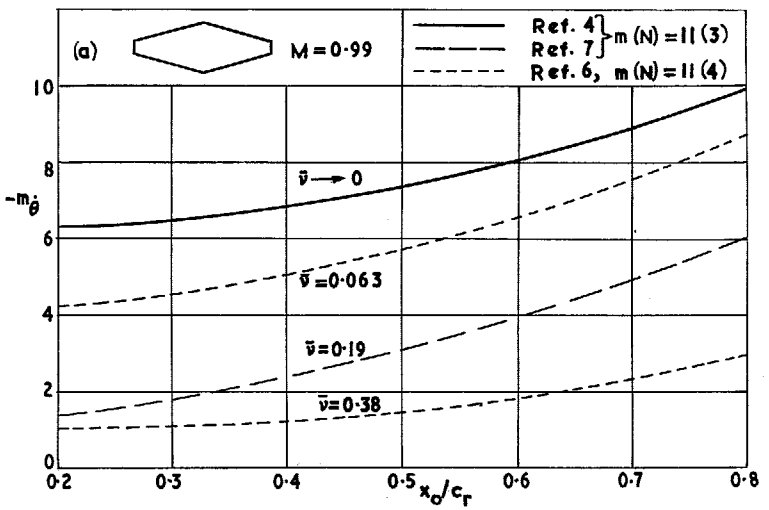

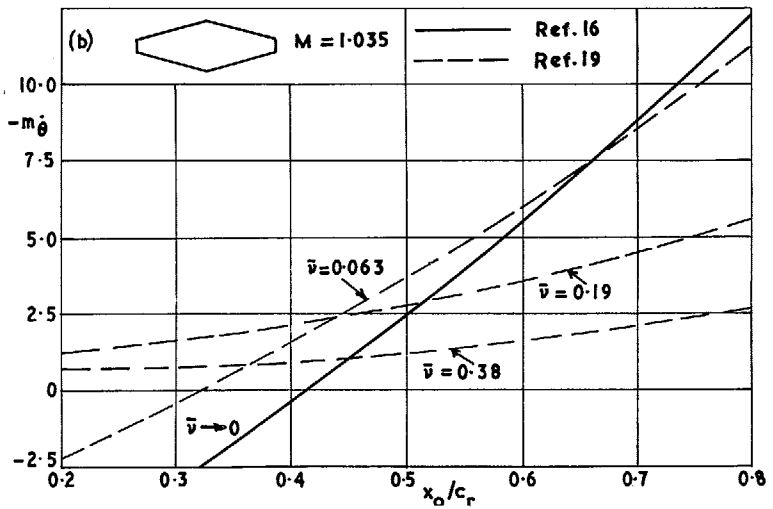

FIG. 30. $-m_{\dot\theta}$ against x_0/c_r for symmetrical tapered wing at $M = 0{\cdot}99$ and $M = 1{\cdot}035$.

THIS DOCUMENT PROVIDED BY THE ABBOTT AEROSPACE
TECHNICAL LIBRARY
ABBOTTAEROSPACE.COM

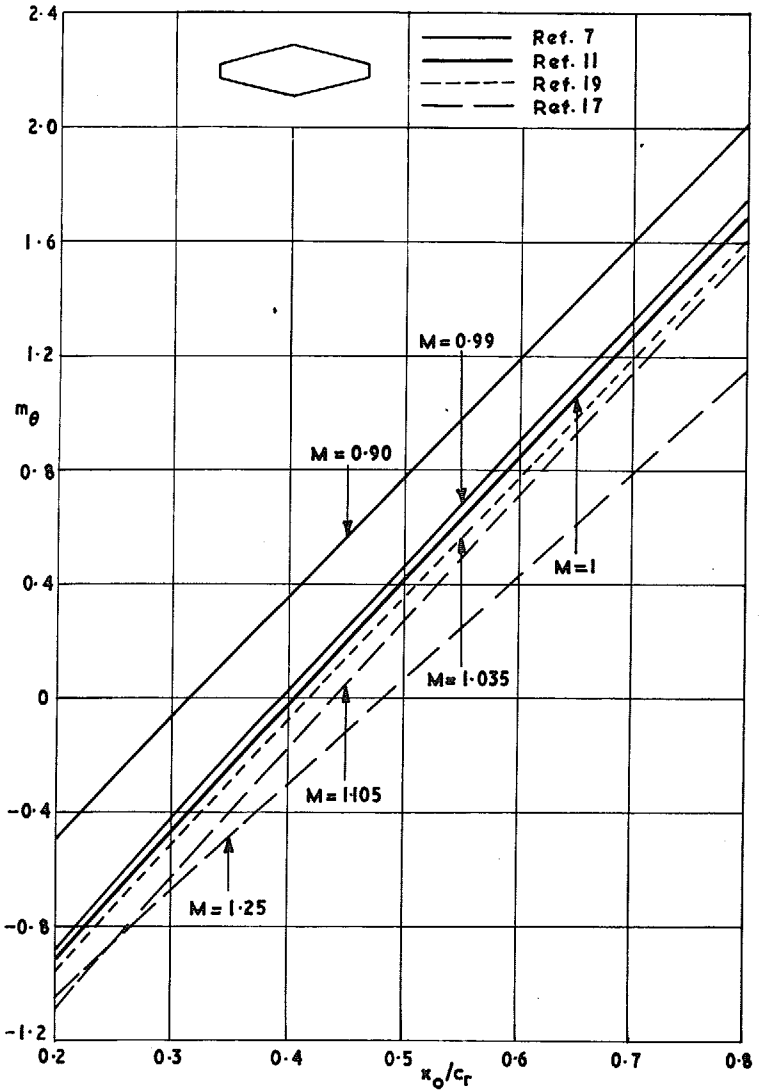

FIG. 31. m_θ against x_0/c_r for symmetrical tapered wing ($\bar{\nu} = 0{\cdot}19$).

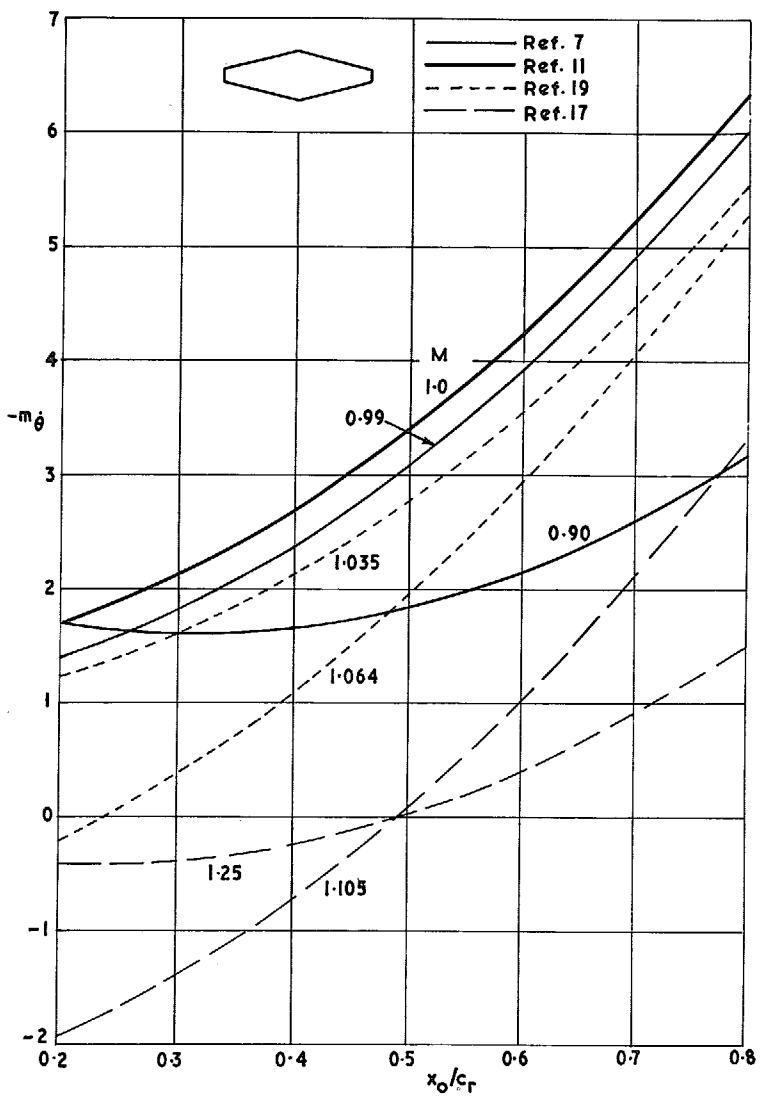

FIG. 32. $-m_{\dot\theta}$ against x_0/c_r for symmetrical tapered wing ($\bar{\nu} = 0{\cdot}19$).

THIS DOCUMENT PROVIDED BY THE ABBOTT AEROSPACE
TECHNICAL LIBRARY
ABBOTTAEROSPACE.COM

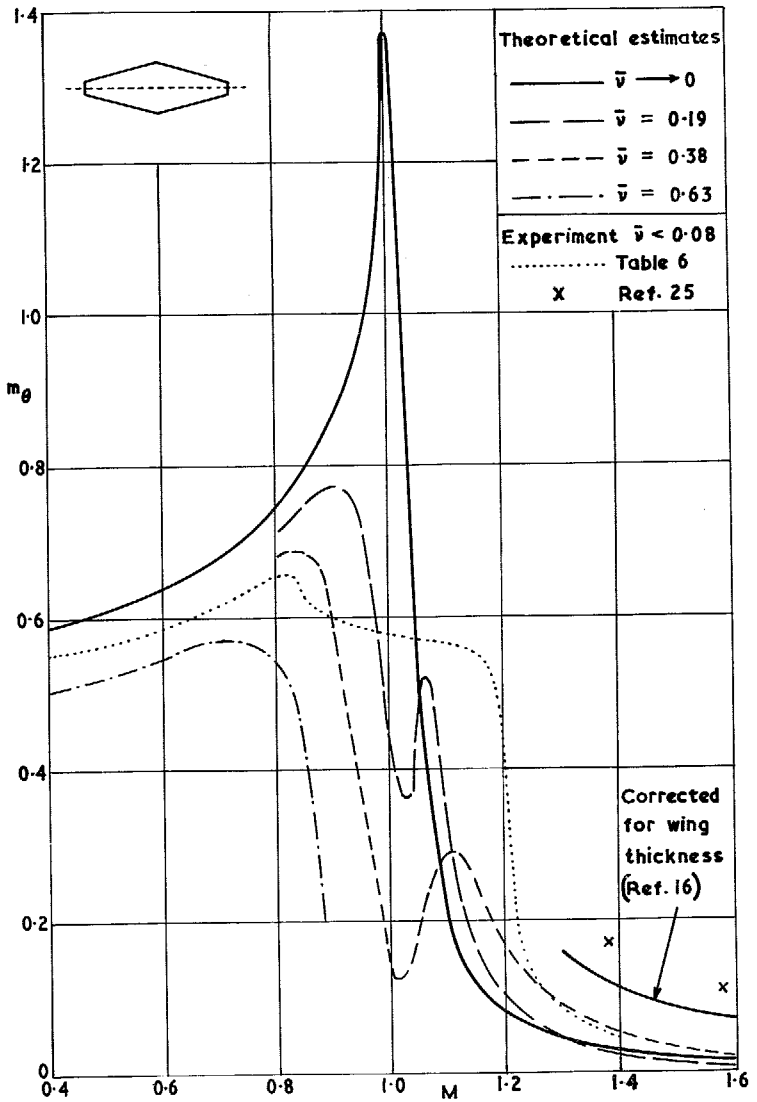

FIG. 33. Digest of theoretical and experimental m_θ for symmetrical tapered wing ($x_0 = 0{\cdot}79\bar{c}$).

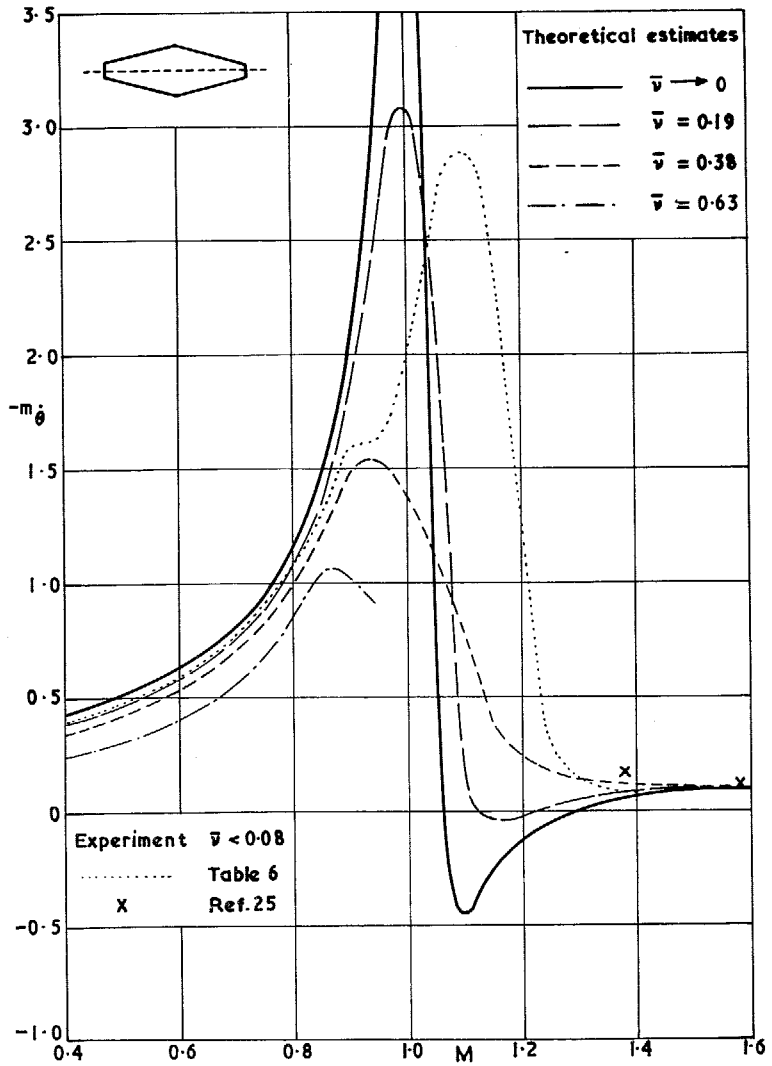

FIG. 34. Digest of theoretical and experimental $-m_{\dot{\theta}}$ for symmetrical tapered wing ($x_0 = 0{\cdot}79\bar{c}$).

Dd. 135646 K5

Printed in Wales for Her Majesty's Stationery Office by Allens Printers (Wales) Limited

THIS DOCUMENT PROVIDED BY THE ABBOTT AEROSPACE
TECHNICAL LIBRARY
ABBOTTAEROSPACE.COM

© *Crown copyright* 1969

Published by
HER MAJESTY'S STATIONERY OFFICE

To be purchased from
49 High Holborn, London W.C.1
13A Castle Street, Edinburgh 2
109 St. Mary Street, Cardiff CF1 1JW
Brazennose Street, Manchester M60 8AS
50 Fairfax Street, Bristol BS1 3DE
258 Broad Street, Birmingham 1
7 Linenhall Street, Belfast BT2 8AY
or through any bookseller

R. & M. No. 3559

S.O. Code No. 23–3559